AD_____

Award Number: W81XWH-06-1-0235

TITLE: Automated Patient Positioning Guided by Cone-Beam CT for Prostate Radiotherapy

PRINCIPAL INVESTIGATOR: Tianfang Li, Ph.D.

CONTRACTING ORGANIZATION: Leland Stanford Junior University
Stanford CA 94305-4125

REPORT DATE: January 2007

TYPE OF REPORT: Annual

PREPARED FOR: U.S. Army Medical Research and Materiel Command
Fort Detrick, Maryland 21702-5012

DISTRIBUTION STATEMENT: Approved for Public Release;
Distribution Unlimited

The views, opinions and/or findings contained in this report are those of the author(s) and should not be construed as an official Department of the Army position, policy or decision unless so designated by other documentation.

REPORT DOCUMENTATION PAGE

Form Approved
OMB No. 0704-0188

Public reporting burden for this collection of information is estimated to average 1 hour per response, including the time for reviewing instructions, searching existing data sources, gathering and maintaining the data needed, and completing and reviewing this collection of information. Send comments regarding this burden estimate or any other aspect of this collection of information, including suggestions for reducing this burden to Department of Defense, Washington Headquarters Services, Directorate for Information Operations and Reports (0704-0188), 1215 Jefferson Davis Highway, Suite 1204, Arlington, VA 22202-4302. Respondents should be aware that notwithstanding any other provision of law, no person shall be subject to any penalty for failing to comply with a collection of information if it does not display a currently valid OMB control number. **PLEASE DO NOT RETURN YOUR FORM TO THE ABOVE ADDRESS.**

1. REPORT DATE *(DD-MM-YYYY)*	2. REPORT TYPE	3. DATES COVERED *(From - To)*
01-01-2007	Annual	01 Jan 06 – 31 Dec 06

4. TITLE AND SUBTITLE
Automated Patient Positioning Guided by Cone-Beam CT for Prostate Radiotherapy

5a. CONTRACT NUMBER

5b. GRANT NUMBER
W81XWH-06-1-0235

5c. PROGRAM ELEMENT NUMBER

6. AUTHOR(S)
Tianfang Li, Ph.D.

E-Mail: tfli@reyes.stanford.edu

5d. PROJECT NUMBER

5e. TASK NUMBER

5f. WORK UNIT NUMBER

7. PERFORMING ORGANIZATION NAME(S) AND ADDRESS(ES)

Leland Stanford Junior University
Stanford CA 94305-4125

8. PERFORMING ORGANIZATION REPORT NUMBER

9. SPONSORING / MONITORING AGENCY NAME(S) AND ADDRESS(ES)
U.S. Army Medical Research and Materiel Command
Fort Detrick, Maryland 21702-5012

10. SPONSOR/MONITOR'S ACRONYM(S)

11. SPONSOR/MONITOR'S REPORT NUMBER(S)

12. DISTRIBUTION / AVAILABILITY STATEMENT
Approved for Public Release; Distribution Unlimited

13. SUPPLEMENTARY NOTES

14. ABSTRACT

Modern radiotherapy equipment is capable of delivering high precision conformal dose distributions to the target. However, the target localization especially for soft-tissue target such as prostate is an issue, because of its possible non-rigid internal motion relative to bony structures or external landmarks. Recently, a new technology of kilo-voltage cone-beam CT (CBCT) has been integrated with the linear accelerator treatment machine. Superior to the common approach based on the two orthogonal images provided by the mega-voltage EPID, CBCT can provide high-resolution three-dimensional (3D) information of the patient in the treatment position. Thus the target localization could be potentially done more accurately without using any implanted fiducials. In practice, however, there is currently still a general lack of efficient method to utilize the 3D CBCT images. In this work, we have developeda clinically practical technique for automatic patient positioning based on the newly emerged CBCT, accounting for the non-rigid motions of the prostate and surrounding structures. A novel deformable registration method has also been developed to improve the positioning accuracy. Furthermore, a low-dose CBCT acquisition protocol is being developed so that a daily use of CBCT becomes possible for prostate patients.

15. SUBJECT TERMS
Prostate Cancer

16. SECURITY CLASSIFICATION OF:			17. LIMITATION OF ABSTRACT	18. NUMBER OF PAGES	19a. NAME OF RESPONSIBLE PERSON
a. REPORT	b. ABSTRACT	c. THIS PAGE			USAMRMC
U	U	U	UU	37	19b. TELEPHONE NUMBER *(include area code)*

Table of Contents

INRTODCUCTION

This postdoctoral traineeship grant (W81XWH-06-1-0235, entitled "Automated Patient Positioning Guided by Cone-Beam CT for Prostate Radiotherapy") was awarded to the principal investigator (PI) for the period of Jan. 1, 2006 to Dec. 31, 2007. This is the annual report for the first funding period (Jan. 1, 2006 – Dec. 31, 2006). The goal of this project is to develop a clinically practical technique for prostate patient positioning based on newly emerged CBCT on-board imaging system. Under the generous support from the U.S. Army Medical Research and Materiel Command (USAMRMC), the PI has gained a tremendous amount of knowledge on prostate cancer and prostate cancer management. The support has also made it possible for the PI to contribute significantly to prostate cancer research. A number of conference and refereed publications have been resulted from the support. In this report, the past year's research activities of the PI are summarized.

BODY

A. Introduction

Modern radiotherapy equipment is capable of delivering high precision conformal dose distributions to the target. However, to precisely locate the target prior to each treatment fraction, especially for soft tissue, is often problematic, due to the non-rigid internal motion of the target relative to bony structures or external landmarks. For this reason, gold-seed implants have been often used, for example in prostate, serving as a surrogate to enhance the visibility of the target in the portal film or the electronic portal imaging device (EPID). Recently, a new technology of kilo-voltage cone-beam CT (CBCT) has been integrated onboard with the linear accelerator (Linac) treatment machine. Superior to the common approach based on the two orthogonal images provided by the mega-voltage EPID, CBCT can offer high-resolution three-dimensional (3D) information of the patient in the treatment position. Thus the target localization could be potentially done more accurately with the aid of the onboard CBCT imager without using any implanted fiducials [1-12]. Although the CBCT technology provides many opportunities, in practice, there is currently a general lack of efficient method to utilize the 3D CBCT images for patient positioning. The two major inherent difficulties in the task of prostate localization are, first, the inter-fraction organ motions are more pronounced at pelvis than other sites, due to the emptying and filling of flexible organs nearby (rectum, bladder and to some extent, small bowel); secondly, the prostate has relatively low contrast resolution in CT images, which is likely to cause more errors in target delineation or localization. A lot of efforts have been made in utilizing CBCT for prostate-target positioning [13-15], for instance, to position using bony landmarks. Since the prostate gland can move independently to the bony structures and its shape may also change, this commonly used positioning technique results in large uncertainties in prostate targeting. Manually matching the prostate target based on the CBCT image is also possible but is time consuming and will introduce significant inter/intra-operator uncertainties.

B. New Patient Positioning Technique

We have developed a novel automated patient positioning technique for prostate cancer patients using deformable image registration. The significant advantages of this technique over traditional method are two-fold. First, it accounts for the complex non-rigid motion of the soft-tissue organs; Secondly, it considers both the prostate target and the organs at risk (OARs) simultaneously, thus a better clinical decision can be made in term of balancing the

displacements of the target and OARs. In brief, the method first registers the 3D CBCT image, acquired in the treatment room, to the 3D planning CT image using B-Spline deformable model, so that a point-to-point correspondence for the patient over the time (the period from planning to treatment) or the "deformation field" can be established. The displacement of every point in the target and sensitive structures are subsequently calculated and used to determine the final couch shifts by a weighted sum.

We have verified our positioning technique using a Varian Trilogy™ system (Varian Medical Systems, Palo Alto, CA) installed in our clinic at Stanford Hospital, which is equipped with a kilo-voltage CBCT imager (see Figure 1). To test the technique, we have also built a pelvis phantom consisting of bladder, prostate, rectum, and bony structures, as illustrated in Figure 2. The phantom was first scanned with a clinical CT (General Electric Medical Systems, Waukesha, WI), with which a four-field 3D conformal treatment plan was generated. After deformation, it was scanned again with both the regular CT and the CBCT. The planning CT was acquired at 120 kV, 380 mA, 2.5mm slice thickness using helical mode, while the positioning CBCT were acquired at 80 mA with other scan parameters kept the same. The position of the "prostate" target was then derived using these images by three different approaches, including the proposed one based on deformable registration, one based on bony anatomy alignment, and one based on minimizing CT-number difference (MCD) via rigid translation of the target [15].

Fig. 1. Varian Trilogy™ oncology system.

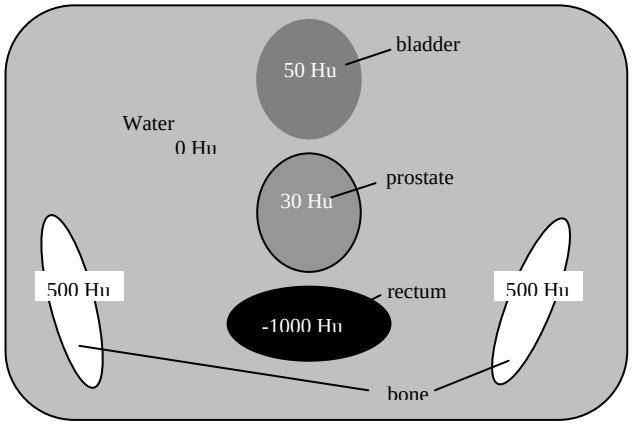

Fig. 2. Sketch of a deformable pelvis phantom.

It was found that both the proposed and the MCD methods showed clear differences from bony anatomy alignment, reflecting the fact that the target had an internal motion independent to the bony structures. However, significant discrepancies were also observed between the proposed and the MCD methods, specifically, 12mm in x, 9mm in y, and 5mm in z axis in this study. Comparing Figures 3(a) and 3(b), we found that the proposed method presented much better accuracy for the target localization. In each of the two figures, positioning parameters were also calculated by using the regular CT images of the deformed phantom instead of CBCT, in which consistent results were achieved by the proposed one (see Figure 3b), while the MCD method generated different parameters (see Figure 3a). One of the reasons for MCD generating varied results when CBCT was replaced by clinical CT for positioning, is because that the clinical CT and the onboard CBCT have observable CT-number difference for the same tissue.

The proposed registration-based CBCT repositioning is quite robust to noise and system errors of the imaging modalities. With this technique, the uncertainties of soft-tissue target localization could be greatly reduced, which ensures conformal dose distribution to be precisely

delivered as planned. This will also enable the implementation of conformal radiotherapy for prostate tumor with much smaller margins than currently applied, leading to less complications and side effects and improved outcome of radiotherapy.

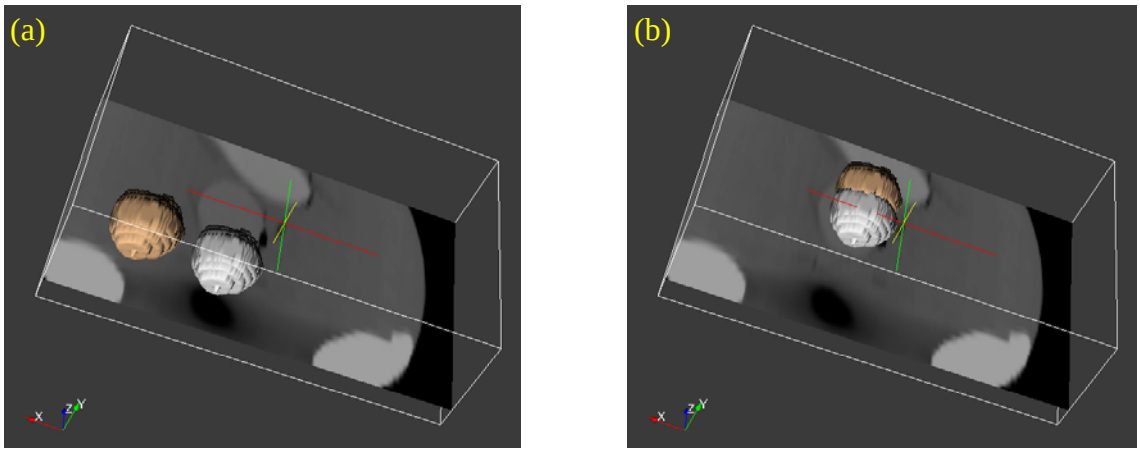

Fig. 3. Positioning with (a) minimum CT-number difference and (b) deformable registration. The box outlines the volumetric image of the phantom in the treatment position. The color contour shows the same target after CBCT-guided repositioning, and the gray contour is the target after regular CT-guided repositioning. The CT-number difference between clinical CT and on-board CBCT resulted in discrepancy in the positioning parameters by this method.

C. Registration Technique Refinement: theoretical investigation

One of the most important issues of using CBCT images is to accurately register it with the planning CT image, which is not only essential to patient positioning, but also critical to various applications such as treatment planning and delivered dose verification or adaptive radiotherapy. Currently, the CBCT imaging system is far from being perfect. Many image degrading factors such as the scatters, the beam hardening, and the approximate reconstruction algorithm etc, adversely affect the final image quality and may subsequently lead to inaccurate registration. Generally speaking, the CBCT 3D image is an artifacts-contaminated image compared with the diagnostic CT image. To improve the registration accuracy, we have been investigating a novel *image space – to – projection space* registration technique. The method has been validated with computer simulation, and clinical studies are under progress.

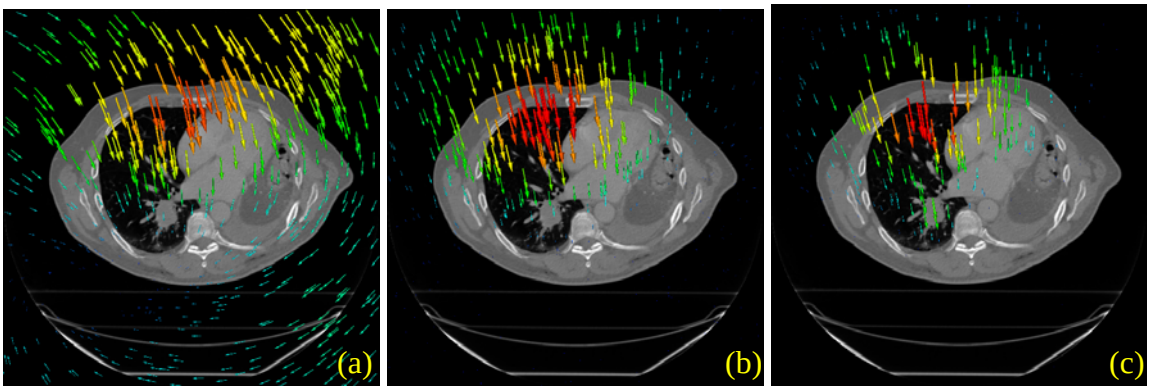

Fig. 4. Deformation field resulted from different registration technique. (a) direct CT to CBCT image registration, where view-aliasing artifacts causes the registration error; (b) CT image to CBCT raw data registration; (c) true deformation field.

Since the reconstruction process often complicates the property of various artifacts, we may avoid the drawback of using low-quality reconstructed image in deriving the motion model by registering the 3D planning CT directly to the CBCT raw data. The unique problem of this method is that the two images being registered are in different spaces, *i.e.* one in the image domain, and the other in the projection domain. We have developed an efficient algorithm for such a registration task using a BSpline model, and one example of the advantage of such method is shown in Figure 4.

To improve the registration further, we are looking for different similarity measurements such as normalized cross correlation and mutual information, to replace the sum of square differences metric that is currently used. It is expected that the new metric will be less influenced by the scatter and other factors inherent in CBCT imaging, and significantly increase the registration accuracy.

D. Exploration of Low-Dose CBCT Imaging

Due to the repeated use of CBCT for a patient, the radiation exposure of the imaging system to patients has been of great concern in radiation oncology. For patient positioning purpose, the strategies to reduce the CBCT radiation exposure that we have come up with during this training period are lowering as much as possible the x-ray tube current and using low number of projections at the same time. The issues associated with low x-ray tube current is mainly the dramatically increased statistical noise, and with low number of projection, the undersampling (view-aliasing) artifacts become prominent in CBCT images. Apparently, simple reduction of the radiation dose results in poor image quality that is not acceptable in most applications. In order to maintain a reasonable image quality or a minimal patient positioning error for this work, we have proposed a generalized CBCT enhancing technique. It is based on the deformable registration of all available information (CT or CBCT images) of the same patient at different time. The extra information borrowed from other images helps to improve the statistics and the data sampling rate as well. As one of the examples we have studied, in Figure 5 it is shown the improvement of the image quality with our enhancing technique for low-dose CBCT acquisition.

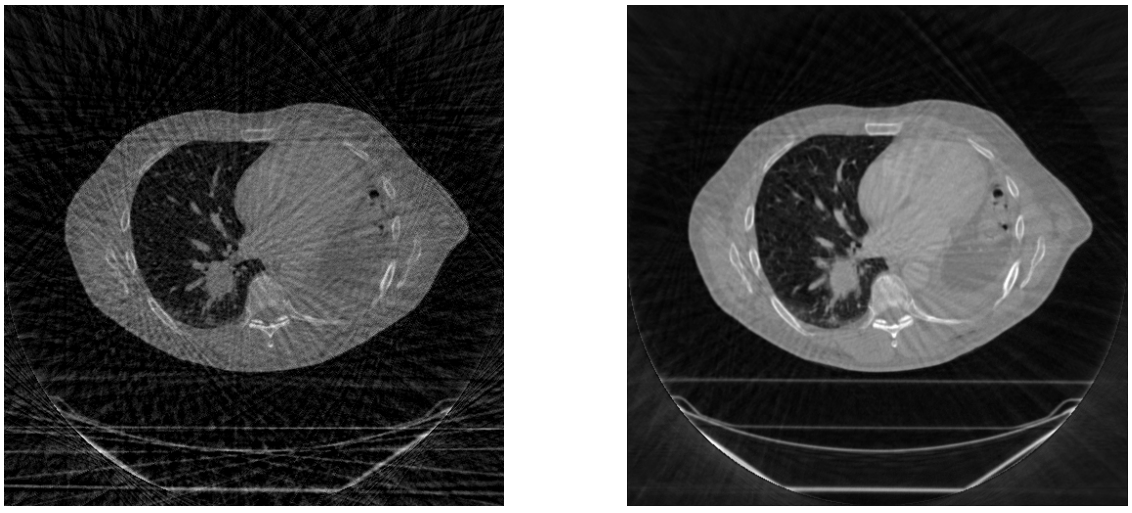

Fig. 5. Left: CBCT image with low number of projections showing undersampling streak artifacts; Right: the improved CBCT image with our enhancing technique based on deformable regirstration.

KEY RESEARCH ACCOMPLISHMENTS

- Developed a new image-to-projection deformable registration algorithm for CBCT/CT image matching, which is more accurate than conventional image-to-image registration method and more robust to various image artifacts such as view-aliasing or truncations.

- Developed and clinically implemented a novel automatic patient positioning strategy, which accounts for non-rigid organ motion, and balance the displacements of various organ structures.

- Improved the CBCT imaging quality and therefore made it possible to use low radiation dose CBCT for daily use, significantly reduced the risk of radiation-induced secondary cancer for patients.

REPORTABLE OUTCOMES

The following is a list of publications resulted from the grant support. Copies of the publication materials are enclosed with this report.

Refereed Journal Publications:

- **T. Li** and L. Xing, "Optimize 4D Cone-Beam CT Acquisition Protocol for External Beam Radiotherapy," International Journal of Radiation Oncology, Biology, Physics, *in press*.
- **T. Li**, A. Koong, and L. Xing, "Enhanced 4D cone-beam CT with inter-phase motion model", submitted to Medical Physics, 2006.

Published Scientific Abstracts:

The PIs' group has also been active in disseminating the research results. The following are some of the presentations given in various national/international meetings.

- **T Li**, E. Schreibmann, A. Koong, Q. Xu, and L. Xing, "Verification of gated radiation therapy using pre-treatment 4D CBCT," International Journal of Radiation Oncology Biology Physics, 66(3), S604, 2006.
- W. Mao**, T. Li**, P. Munro, M. Chao, and L. Xing, "Individualizing 4D CBCT acquisition protocol for external beam radiotherapy," International Journal of Radiation Oncology Biology Physics, 66(3), S146-S147, 2006.
- **T. Li**, E. Schreibmann, A. Koong, Q. Xu, R. Hamilton and L. Xing, "Verification of Gated Radiation Therapy Using Pre-Treatment Four-Dimenstional Cone-Beam CT," International Journal of Radiation Oncology Biology Physics, 66(3), S604, 2006.
- L. Xing, A. de la Zerd, M. Cao, **T. Li**, B. Armbrush, Y. Yang, P. Lee, T. Pawlicki, S. Hancock and C. King, "On-Board Volumetric CT-based Adaptive IMRT For Improved Prostate Cancer Treatment," International Journal of Radiation Oncology Biology Physics, 66(3), S624-S625 , 2006.

- M. Chao, E. Schreibmann, **T. Li**, A. Koong, K.A. Goodman and L. Xing, "Automatic Contouring in 4D Radiation Therapy," International Journal of Radiation Oncology Biology Physics, 66(3), S649, 2006.
- E. Elder, E. Schreibmann, **T. Li**, T. Fox, L. Xing, J. Crocker and J. Landry, "Registration of 4D CBCT and 4D CT for Extracranial Stereotactic Treatments," International Journal of Radiation Oncology Biology Physics, 66(3), S651, 2006.
- P. Peng, M. Chao, Q. Le, **T. Li**, A. Hsu, T.A. Pawlicki and L. Xing, "Auto Contour Mapping in CBCT for Adaptive Therapy Treatment Planning," International Journal of Radiation Oncology Biology Physics, 66(3), S651-S652, 2006.
- **T. Li**, L Xing, P. Munro et al, "4D Cone-Beam CT (CBCT) Using An On-Board Imager," Med. Phys. 33, 2234, 2006.
- M. Chao, **T. Li**, and L. Xing, "Enhanced 4D CBCT Imaging for Slow-Rotating On-Board Imager ," Med. Phys. 33, 2269, 2006.
- M. Chao, E. Schreibmann, **T. Li**, and L. Xing, "Knowledge-Based Auto-Contouring in 4D Radiation Therapy," Med. Phys. 33, 2171, 2006.

CONCLUSIONS

Despite the well-appreciated fact that onboard CBCT system can provide 3D anatomical information of a patient in the treatment position, its clinical applications have been hindered by the deficiencies in image quantitative accuracy and by the lack of a comprehensive image analysis procedure. This is evidenced by that very few institutions are using CBCT routinely for prostate cancer treatment. A challenge here is how to achieve automatic and accurate patient positioning with consideration of the non-rigid motions of the prostate and surrounding structures.

In this work, a novel patient positioning technique is developed and its utility for prostate cancer treatment is evaluated. Various factors affecting the final positioning decisions are addressed. Specifically, in dealing with the quantitative errors in the 3D or 4D images provided by current CBCT system, a more reliable deformable registration algorithm mapping from image space to projection space has been investigated and has shown very promising results. Furthermore, a low-dose CBCT imaging protocol is being developed, based on an image enhancing technique that we have developed for the CBCT imaging system, which makes it possible to employ CBCT on a daily basis without increasing the risk of radiation-induced secondary cancer or compromising the patient treatment outcome. With more evaluations, the automatic patient positioning technique will soon be part of routine practice at Stanford University Hospital. The data and experiences we accumulated in this project are well documented, and serve as a good reference for effectively utilizing CBCT imager, and will definitely enhance the outlook of the onboard CBCT in guiding radiation therapy as a whole.

REFERENCES:

1. L. Xing, B. Thorndyke, E. Schreibmann, Y. Yang, T. Li, G. Luxton, and A. Koong, "Overview of image guided radiation therapy," *Medical Dosimetry*, **31**(2), 91-112 (2006).
2 R. I. Berbeco, S. B. Jiang, G. C. Sharp, G. T. Chen, H. Mostafavi, and H. Shirato, "Integrated radiotherapy imaging system (IRIS): design considerations of tumour tracking with linac gantry-mounted diagnostic x-ray systems with flat-panel detectors," *Phys Med Biol* **49**(2), 243-255 (2004).
3 M. J. Ghilezan, D. A. Jaffray, J. H. Siewerdsen, M. Van Herk, A. Shetty, M. B. Sharpe, S. Zafar Jafri, F. A. Vicini, R. C. Matter, D. S. Brabbins, and A. A. Martinez, "Prostate gland motion assessed with cine-magnetic resonance imaging (cine-MRI)," *Int J Radiat Oncol Biol Phys* **62**(2), 406-417 (2005).

4 D. Letourneau, A. A. Martinez, D. Lockman, D. Yan, C. Vargas, G. Ivaldi, and J. Wong, "Assessment of residual error for online cone-beam CT-guided treatment of prostate cancer patients," *Int J Radiat Oncol Biol Phys* **62**(4), 1239-1246 (2005).
5 T. R. Mackie, J. Kapatoes, K. Ruchala, W. Lu, C. Wu, G. Olivera, L. Forrest, W. Tome, J. Welsh, R. Jeraj, P. Harari, P. Reckwerdt, B. Paliwal, M. Ritter, H. Keller, J. Fowler, and M. Mehta, "Image guidance for precise conformal radiotherapy," *Int J Radiat Oncol Biol Phys* **56**(1), 89-105 (2003).
6 R. Mohan, X. Zhang, H. Wang, Y. Kang, X. Wang, H. Liu, K. K. Ang, D. Kuban, and L. Dong, "Use of deformed intensity distributions for on-line modification of image-guided IMRT to account for interfractional anatomic changes," *Int J Radiat Oncol Biol Phys* **61**(4), 1258-1266 (2005).
7 H. Shirato, S. Shimizu, T. Kunieda, K. Kitamura, M. van Herk, K. Kagei, T. Nishioka, S. Hashimoto, K. Fujita, H. Aoyama, K. Tsuchiya, K. Kudo, and K. Miyasaka, "Physical aspects of a real-time tumor-tracking system for gated radiotherapy," *Int J Radiat Oncol Biol Phys* **48**(4), 1187-1195 (2000).
8 S. L. Meeks, J. F. Harmon, Jr., K. M. Langen, T. R. Willoughby, T. H. Wagner, and P. A. Kupelian, "Performance characterization of megavoltage computed tomography imaging on a helical tomotherapy unit," *Med Phys* **32**(8), 2673-2681 (2005).
9 J. Pouliot, A. Bani-Hashemi, J. Chen, M. Svatos, F. Ghelmansarai, M. Mitschke, M. Aubin, P. Xia, O. Morin, K. Bucci, M. Roach, 3rd, P. Hernandez, Z. Zheng, D. Hristov, and L. Verhey, "Low-dose megavoltage cone-beam CT for radiation therapy," *Int J Radiat Oncol Biol Phys* **61**(2), 552-560 (2005).
10 K. M. Langen, S. L. Meeks, D. O. Poole, T. H. Wagner, T. R. Willoughby, P. A. Kupelian, K. J. Ruchala, J. Haimerl, and G. H. Olivera, "The use of megavoltage CT (MVCT) images for dose recomputations," *Phys Med Biol* **50**(18), 4259-4276 (2005).
11 C. F. Elder, W. K. Rebecca, D. Letourneau, D. A. Jaffray, J. Bissonnette, A. Bezjak, P. Greg, W. Elizabeth, M. Carol, M. Michael, S. Michael, and G. Mary, "Towards a one-step scan and treat process for palliative radiotherapy - a potential application for cone beam computerized tomography (CBCT)," *Int J Radiat Oncol Biol Phys* **63**(2), S440 (2005).
12 M. Oldham, D. Letourneau, L. Watt, G. Hugo, D. Yan, D. Lockman, L. H. Kim, P. Y. Chen, A. Martinez, and J. W. Wong, "Cone-beam-CT guided radiation therapy: A model for on-line application," Radiother Oncol 75(3), 271-278 (2005).Jaffray DA, Drake DG, Moreau M, *et al*. A radiographic and tomographic imaging system integrated into a medical linear accelerator for localization of bone and soft-tissue targets. *Int JRadiat Oncol Biol Phys* **45**:773-789 (1999).
13. van Herk M, Jaffray D, Betgen A, *et al*. First clinical experience with cone-beam CT guided radiation therapy: evaluation of dose and geometric accuracy. *Int J Radiat Oncol Biol Phys* **60**:S196 (2004).
14. D. Rueckert, L.I. Sonoda, C. Hayes, D.L. Hill, M.O. Leach, and D.J. Hawkes, "Nonrigid registration using free-form deformations: application to breast MR images". *IEEE Transactions Medical Imaging* **18**(8): 712-721 (1999)
15 Court LE, Dong L. Automatic registration of the prostate for computed-tomography-guided radiotherapy. *Med Phys* **30**:2750-2757 (2003).

Appendix I. Copy of manuscripts

ARTICLE IN PRESS

Int. J. Radiation Oncology Biol. Phys., Vol. xx, No. x, pp. xxx, 2006
Copyright © 2006 Elsevier Inc.
Printed in the USA. All rights reserved
0360-3016/06/$–see front matter

ELSEVIER

doi:10.1016/j.ijrobp.2006.10.024

CLINICAL INVESTIGATION

OPTIMIZING 4D CONE-BEAM CT ACQUISITION PROTOCOL FOR EXTERNAL BEAM RADIOTHERAPY

TIANFANG LI, PH.D., AND LEI XING, PH.D.

Department of Radiation Oncology, Stanford University School of Medicine, Stanford, CA

Purpose: Four-dimensional cone-beam computed tomography (4D-CBCT) imaging is sensitive to parameters such as gantry rotation speed, number of gantry rotations, X-ray pulse rate, and tube current, as well as a patient's breathing pattern. The aim of this study is to optimize the image acquisition on a *patient-specific* basis while minimizing the scan time and the radiation dose.

Methods and Materials: More than 60 sets of 4D-CBCT images, each with a temporal resolution of 10 phases, were acquired using multiple-gantry rotation and slow-gantry rotation techniques. The image quality was quantified with a relative root mean-square error (RE) and correlated with various acquisition settings; specifically, varying gantry rotation speed, varying both the rotation speed and the number of rotations, and varying both the rotation speed and tube current to keep the radiation exposure constant. These experiments were repeated for three different respiratory periods.

Results: With similar radiation dose, 4D-CBCT images acquired with low current and low rotation speed have better quality over images obtained with high current and high rotation speed. In general, a one-rotation low-speed scan is superior to a two-rotation double-speed scan, even though they provide the same number of projections. Furthermore, it is found that the image quality behaves monotonically with the relative speed as defined by the gantry rotation speed and the patient respiratory period.

Conclusions: The RE curves established in this work can be used to predict the 4D-CBCT image quality before a scan. This allows the acquisition protocol to be optimized individually to balance the desired quality with the associated scanning time and patient radiation dose. © 2006 Elsevier Inc.

Image-guided radiotherapy, Four-dimensional cone-beam CT, Optimization.

INTRODUCTION

Onboard cone-beam computed tomography (CBCT) imaging provides a convenient means for accurate patient setup and dose verification (1–8). However, when used for thorax or upper abdomen imaging, motion artifacts appear in the reconstructed images because of intrascanning organ motion within the field of view (FOV). According to the International Electric Commission recommendation, onboard CBCT systems have a limited gantry rotation speed of 60 s per round. A complete scan therefore consists of projection data from 10 to 20 respiratory cycles of the patient, resulting in large amount of inconsistency in the CBCT projection data. Reconstruction algorithms based on theories of static object lead to images that are significantly deteriorated by motion artifacts. Because of the prolonged scanning time, these motion-induced adverse effects in CBCT are much more severe than those seen in conventional CT scans (9). The artifacts not only blur the image, but also inhibit direct use of CBCT for dose calculation (10–12).

Four-dimensional (4D) CBCT, or respiration-correlated CBCT, groups the acquired projection data into several bins as according to their respiratory phases. Each phase bin is then reconstructed independently to obtain a volumetric image corresponding to that specific phase (13–15). 4D-CBCT not only greatly reduces the motion artifacts presented in each of these phase-resolved images, but also provides the dynamic information of the patient anatomy, which is absent in the three-dimensional (3D) case, and could be very useful in future 4D radiotherapy (1).

Because the total amount of projections acquired during a 4D-CBCT scan is divided into several phase groups, the number of projections available for each image reconstruc-

Reprint requests to: Lei Xing, Ph.D., Stanford University School of Medicine, Department of Radiation Oncology, 875 Blake Wilbur Drive, Stanford, CA 94305-5847. Tel: (650) 498-7896; Fax: (650) 498-4015; E-mail: lei@reyes.stanford.edu

This work was supported in part by grants from the Department of Defense (W81XWH-06-1-0235), the American Cancer Society (RSG-01-022-01-CCE) and Komen Breast Cancer Foundation (BCTR0504071).

Acknowledgment—We wish to thank A. Koong, K. Goodman, B. Loo, G. Luxton, T. Pawlicki, P. Maxim, E. Schreibmann, R. Wu, and R. Wiersma from Stanford University, and P. Munro, M. Svatos, S. Johnson, C. Zankowski, and R. Wicha from Varian Medical Systems for useful discussions.

Conflict of interest: none.

Received June 10, 2006, and in revised form Oct 3, 2006. Accepted for publication Oct 9, 2006.

ARTICLE IN PRESS

tion becomes much less than in the regular 3D-CBCT case. As known from theory, the number of projections needed to avoid undersampling artifacts is inversely proportional to the reconstructed voxel size (16). An insufficient number of projections will lead to severe view-aliasing artifacts. To increase the number of projections for each phase, two strategies that can be employed are: slowing down the gantry rotation speed (SGR) and multiple gantry rotations (MGR). In addition to the gantry rotation speed and the number of gantry rotations, the quality of 4D-CBCT images is also sensitive to parameters such as the X-ray pulse rate, the tube current, and the patient's breathing pattern. These parameters constitute a multidimensional space, making the optimal 4D-CBCT protocol intractable. To balance the tradeoff between image quality, scan time, and patient radiation dose, a patient-specific 4D-CBCT acquisition protocol is highly desirable. This issue is systematically studied in this work, with the goal of fully understanding the influences of these various scanning parameters to optimize 4D-CBCT data acquisition protocol.

METHODS AND MATERIALS

4D-CBCT data acquisition system

An Acuity simulator (Varian Medical Systems, Palo Alto, CA) was used in this work for all CBCT imaging. In the case of regular 3D-CBCT simulation, a gantry rotation speed of 8°/s is used. The X-ray tube operates at 125 kVp and 80 mA with a pulse width at each projection angle of 9 ms when no bow-tie filter is used. The pulse width is increased to 25 ms if a bow-tie filter is used to maintain similar photon statistics. The data are acquired at ~15 frames/s and a full rotation (slightly more than 360°) consists of about 685 projections corresponding to an angle interval of about 0.5°. The radiation dose of a one-rotation CBCT scan at isocenter is approximately 4.0 cGy. The dimension of each acquired projection image is 397.3 mm × 298.0 mm, containing 1,024 × 768 pixels. With a source-to-axis distance of 100 cm and source-to-detector distance of 150 cm, the field of view is around 25 cm in diameter in the transverse plane for a full-fan mode. This can be close to 50 cm if a half-fan mode is employed (by shifting the flat-panel detector laterally). Here it should be noted that the half-fan mode generally results in inferior image quality when compared with that obtained with full-fan mode if all other acquisition parameters are maintained the same, and is a consequence of the loss of the data redundancy as is in the full-fan mode. However, for regions such as the thorax, a full-fan mode may result in truncated images, which are not appropriate for dose calculation. Thus the half-fan mode is preferred when a large field of view is required, and this mode is therefore used in this work.

To generate the 4D image sets, the acquired CBCT projections must be sorted into a number of bins according to their specific respiratory phases. The phase information of each projection can be obtained with the aid of a motion tracking system, for example, the Real-time Position Management system (Varian Medical Systems) as done in 4D-CT acquisition with conventional diagnostic CT scanners (17–25), or alternatively, it can be achieved by analyzing the acquired raw data in the projection space (26). In the latter, one or more CT-opaque fiducials are placed on the patient skin and the locations of the fiducials in the projections are detected by a computer searching algorithm. The coordinate of the fiducial is recorded as a function of the gantry angle, revealing the motion status of the object for each projection. In this work, the projection-space approach is used. Figure 1 shows an example of such a plot for the periodically moving phantom. The projections are phase-tagged according to the resultant sinusoidal curve, and sorted into 10 phase groups. The data in each phase bin are then reconstructed independently using a Feldkamp algorithm with a pixel size of 0.5 mm × 0.5 mm in the cross-section plane and a slice thickness of 1.0 mm.

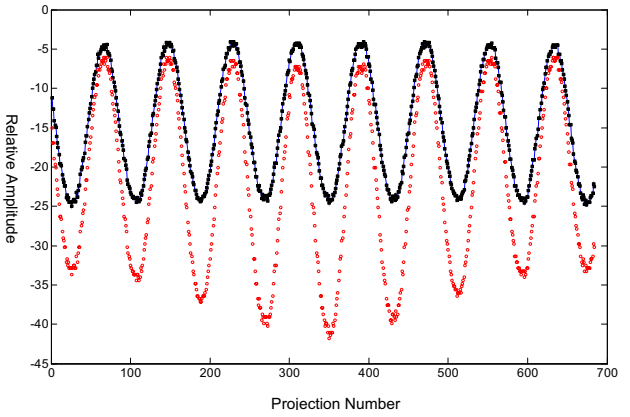

Fig. 1. An example of the projection-space phase tracking used in this work. The black solid squares and the red open circles represent the positions of the fiducial marker in the real world coordinate system and projection space, respectively. The sinusoidal curve obtained from cone-beam computed tomography projections can be used to determine the phase of each projection.

Motion phantom

To investigate the influence of various scanning parameters on the quality of 4D-CBCT, a motion phantom was constructed. The motion phantom consisted of a commercial CT calibration phantom CatPhan 600 (The Phantom Laboratory, Inc., Salem, NY) that is placed on top of a platform capable of sinusoidal motion along three directions: the phantom moved with the maximal displacements 5.5 cm in superoinferior direction, 1.5 cm in anteroposterior direction, and 0.2 cm in lateral direction. The period of the motion was continuously adjustable in the range of 0.5 s–1 min. In this work, three different periods were used to study the effects of breathing cycle on the image quality, which were 3.37 s, 4.59 s, and 6.53 s. 4D-CBCT images of the motion phantom were acquired using SGR or MGR methods as described in the following section. All 4D data acquisitions were using X-ray tube current of 10 mA unless otherwise stated. For comparison, three additional scans, with the phantom "frozen" at the "peak-inspiration," "mid-expiration" and "peak-expiration" phases, were obtained as well using the standard 3D-CBCT protocol (gantry rotation speed at 8°/s, X-ray tube current and voltage at 80 mA and 125 kVp, respectively). The three scans served as our "standards" for these phases.

4D-CBCT image analysis

Because the images in this work involve significant artifacts, a common metric such as contrast-to-noise ratio (CNR), defined as $CNR = |<\bar{S}_1 - \bar{S}_2>|/\sigma$, may not be suitable, in the sense that a high CNR output may not represent a better image. For example, dark streak artifacts may accidentally decrease the mean value of

$\bar{S}_2$, leading to a high CNR value. Thus the CNR metric may highly depend on the selected regions of interest. To have a more robust and accurate assessment of the images obtained using different CBCT settings, a "relative root mean square error" (denoted by *RE*) is chosen as the figure of merit of the image quality, which is defined as

$$RE = \left(\sum_i (S_{4D}(i) - S_0(i))^2 \Big/ \sum_i S_0^2(i) \right)^{1/2}, \quad (1)$$

where S_{4D} denotes the 4D single-phase image, and S_0 is the standard 80-mA 3D-CBCT images of the phantom frozen at the same phase. The summation runs over all voxels of the images. In Eq. 1, S_0 image is used as the "gold standard," and the mean square error between the 4D images and the gold standard is normalized to the mean square of the true intensity.

Slow-gantry rotation strategy

A sufficient number of projections must be collected for each phase to remove the view-aliasing artifacts in 4D-CBCT. One way to achieve this is to slow down the gantry rotation. In this way, the number of breathing cycles covered by a full rotation is increased, leading to more projections in each phase group. Figure 2 is a sketch illustrating the relationship between the gantry rotation schemes and the breathing. The dark areas represent the available projections that belong to the same phase group.

To examine the influence of gantry rotation speed on the resultant image quality, scans were made of the motion phantom for eight gantry rotation speeds ranging from 8°/s to 1°/s. All other system variables were kept constant with the X-ray tube current and voltage in these eight scans being held at 10 mA and 125 kVp, respectively. This increased the total number of projections from about 680 for 8°/s speed to about 5,440 for 1°/s speed. Consequently, the number of projections in each phase bin increased by ~8 times. The resultant 4D-CBCT images were then analyzed using the RE metric as defined in Eq. 1.

Another important quantity for SGR 4D acquisition is the relation between image quality and the associated radiation exposure. For a constant X-ray pulse width, the radiation dose is directly proportional to the number of projections (beam-on time) and essentially linear to the X-ray tube current. Hence a scan with a rotational speed of 1°/s at 10 mA current will result in a similar amount of radiation as a scan with a 2°/s rotation speed at doubled the tube current. To investigate this image quality–tube current relationship, 4D-CBCT images of the motion phantom were acquired for 1°/s-10 mA, 2°/s-20 mA, 4°/s-40 mA, 5°/s-50 mA, and 8°/s-80 mA, for each of the three motion periods mentioned previously. These scanning schemes deliver a similar radiation dose to the phantom. A quantitative comparison of the 4D images was carried out.

Multiple-gantry rotation strategy

An alternative to SGR is MGR 4D acquisition, in which the gantry now rotates multiple times back and forth. As with SGR, the projections of the same phase are again collected and used for 4D-CBCT image reconstruction. The MGR acquisition scheme in relation to the breathing pattern is sketched in Fig. 2c. As shown, both SGR and MGR strategies lead to an increase in the number of projections over conventional CBCT (Figs. 2b, 2c); however, the angular distribution of the projections of a given phase group is very different. In SGR, the projections belonging to a particular breathing phase are regularly distributed in the angular space, whereas in MGR, two or more rotations lead to the projection becoming irregular. As a result, now there is a chance that, during the multiple gantry rotations, projections at the same phase and gantry angle may occur more than once, leading to redundancy of the data and resulting in less effective 4D-CBCT reconstruction. The angular overlap or partial overlap of the projection data can, in principle, be avoided/reduced by properly selecting the initial phase of the two (or multiple) scans. Generally, as illustrated in Fig. 2d, the chance for two successive scans to overlap is minimal when the gantry moves in opposite directions. One can imagine that if two scans are in the same direction, at every angle, the two projections from the two scans may be at same phase in the extreme case. This scenario will never happen if the two scans are in opposite directions. Two-rotation MGR scans with the gantry "back and forth" were performed for each of the previously mentioned three motion periods and the results were compared with that obtained using SGR. To maintain a constant radiation exposure, the gantry rotation speed in the MGR approach was increased by a factor of two as compared with that of a single rotation scan.

Relative gantry speed

Four-dimensional-CBCT image quality depends not only on the gantry rotation speed, but also on the patient respiratory pattern. This suggests that a *patient-specific* setting might be needed to achieve a similar quality of 4D-CBCT images. Here we propose a new measure of *relative speed* to combine the two variables of gantry rotation and patient respiration, which is defined as follows

$$\textit{Relative Speed} = \textit{Respiratory Period}(s) \times \textit{Gantry Rotation Speed}(\deg/s). \quad (2)$$

Relative speed has a unit of degree, which is the spanned angle of the CBCT scan during the time of one respiratory cycle.

The data acquired in these studies, for different motion periods and different scanning speed at constant X-ray tube current (10 mA) and voltage (125 kVp), were reanalyzed to illustrate the utility of the new concept in optimizing the 4D-CBCT image acquisition protocol on a patient-specific basis.

RESULTS

4D-CBCT image quality as a function of gantry rotation speed

Four-dimensional-CBCT images acquired with eight different gantry rotation speeds and constant X-ray tube current (10 mA) for the phantom moving at a period of 3.37 s are summarized in Fig. 3. From the top-left to the bottom-middle, the images correspond to gantry rotation speeds from 8°/s to 1°/s. Without loss of generality, only the phase 0% images of the 4D-CBCT acquisitions are compared here. Note that all other imaging parameters such as the tube current and voltage were the same for all the eight scans. The golden standard image (obtained with a standard 3D-CBCT protocol and without motion) is also shown at the bottom right in Fig. 3. As expected, it is found that the image quality improves with decreasing gantry rotation speeds. Similar trends were also observed for the phantom moving with the other two periods (4.93 s and 6.53 s).

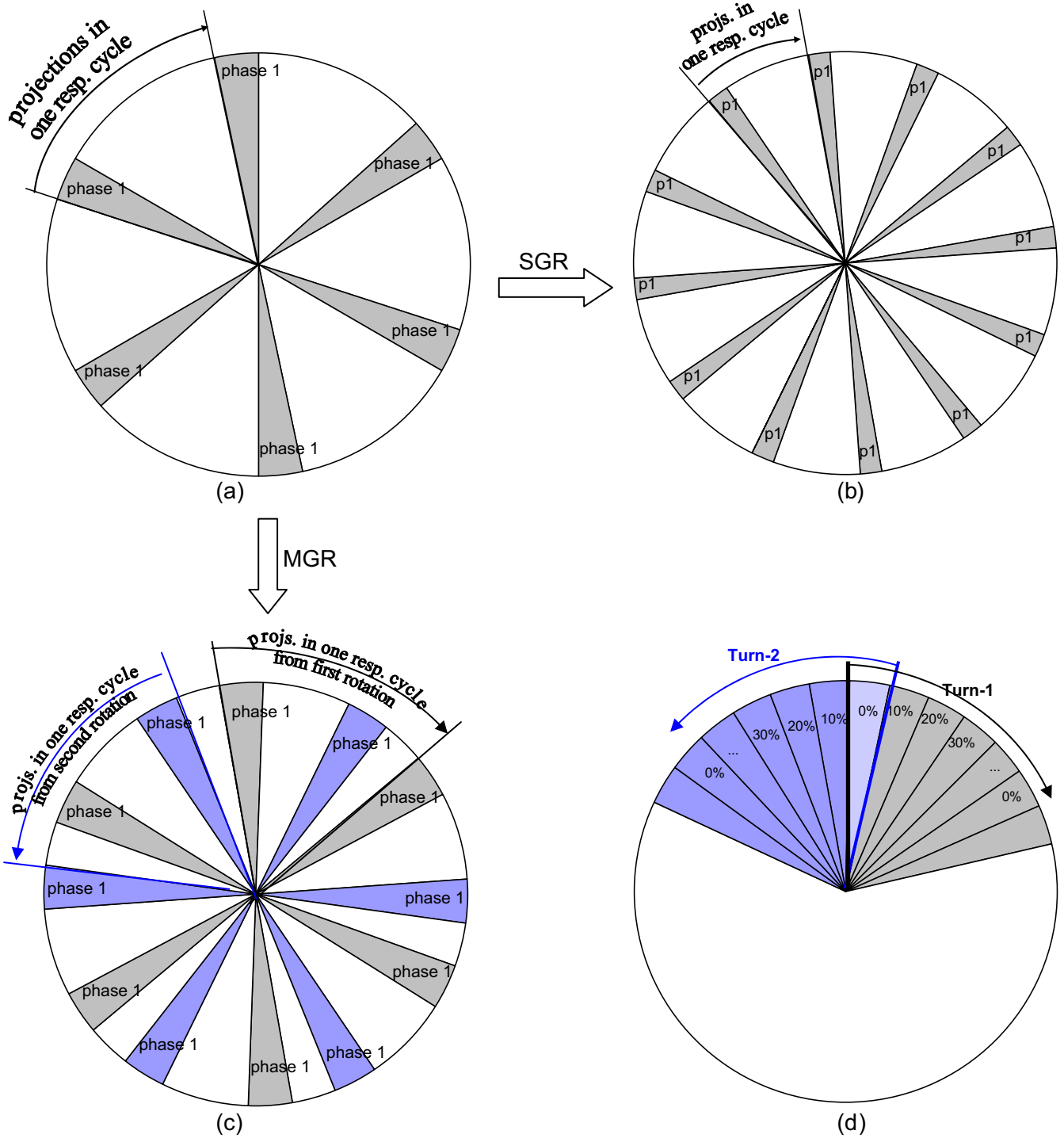

Fig. 2. Illustration of four-dimensional cone-beam computed tomography acquisitions with gantry rotation speed (SGR) and multiple gantry rotations (MGR) methods. The shadow in the diagrams represents the projections available for reconstruction of one particular phase. (a) Single rotation with rotation speed of a conventional three-dimensional scan, in which the number of projections in a phase bin is relatively small; (b) with SGR, a scan expands more respiratory cycles, hence more projections of the same phase can be collected; (c) with MGR, the number of projections in a phase group increases as shown by the gray and blue shadow; (d) the phase distribution in two successive rotations of the MGR method. Note that if two projections overlap at a particular angle, for example, for 0% phase, the projections at neighbor angles will be in different phases because the two rotations are in opposite directions.

The quantitative relation between image quality and gantry rotation speed was analyzed using the image metric of REs and the results were plotted in Fig. 4. For all three respiratory periods, the relative errors are found to increase with increasing gantry rotation speeds, indicating a drop in the image quality. Also from Fig. 4, it is seen that at a given

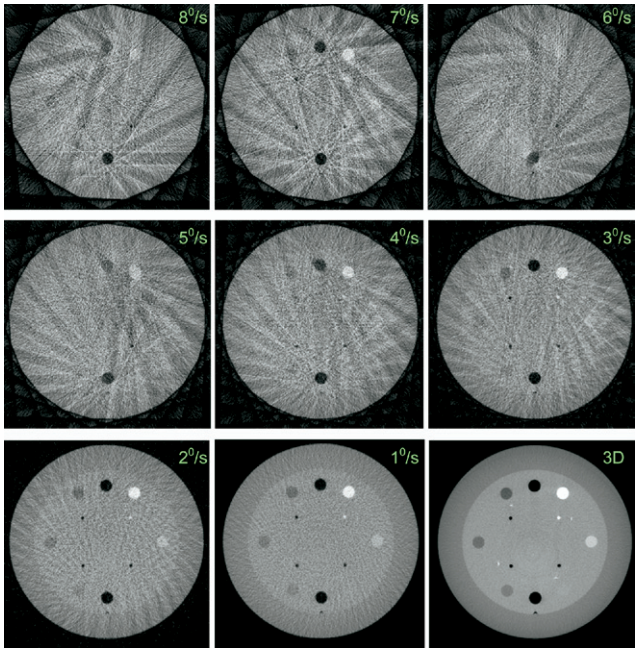

Fig. 3. From the top-left to the bottom-right are the four-dimensional cone-beam computed tomography (4D-CBCT) images of phase 0% obtained by varying the gantry rotation speed from 8°/s to 1°/s, and the three-dimensional CBCT images of the phantom "frozen" at the same phase. All 4D-CBCT were acquired with X-ray tube current of 10 mA.

gantry rotation speed, the image quality improves (smaller REs) with increasing phantom velocities. This is not surprising because a full scan at fast phantom speed will contain more respiratory cycles, leading to a reduction of the gap (Fig. 2) between the projections of same phase in two successive cycles, hence less view-aliasing artifacts. To help visualize this effect, Fig. 5 shows the 0% phase images obtained for the three different motion modes with the same gantry rotation speed of 2°/s.

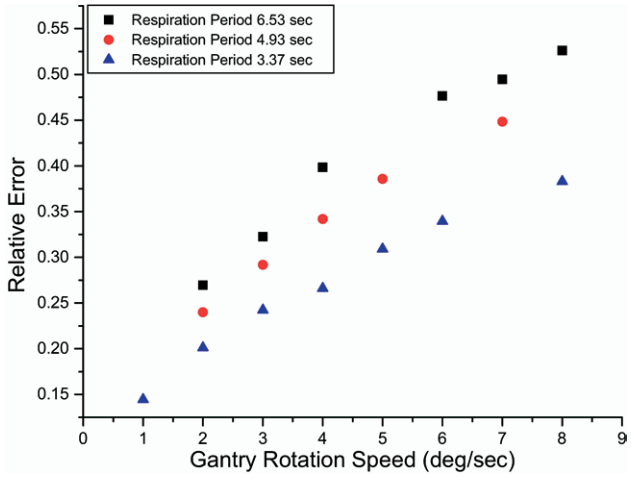

Fig. 4. Relation between relative root mean-square error and gantry rotation speed for three motion modes with periods of 3.37 s, 4.93 s, and 6.53 s, respectively.

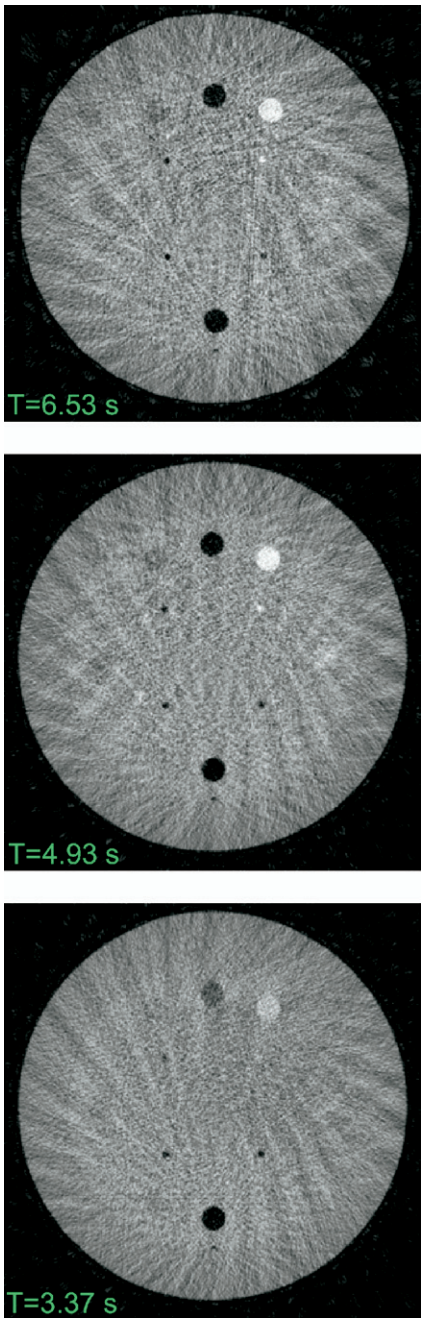

Fig. 5. Four-dimensional cone-beam computed tomography images of phase 0% obtained at the same gantry rotation speed of 2°/s, but different phantom motion periods.

SGR acquisition under the condition of a constant radiation exposure

As mentioned previously, the photon flux, noise level and patient radiation exposure are all related to the tube current. This is investigated by comparison of the 0% phase 4D images for scans of 8°/s at 80 mA, 5°/s at 50 mA, 4°/s at 40 mA, 2°/s at 20 mA, and 1°/s at 10 mA. Because the radiation exposure is approximately proportional to the tube current, scans with these eight settings deliver a similar level of radiation dose to the phantom. Again, the image metric of RE was employed to quantify the difference

ARTICLE IN PRESS

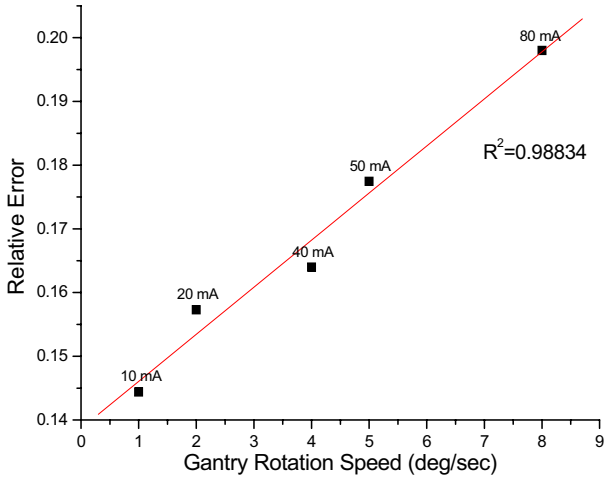

Fig. 6. The effects of increasing tube current and gantry rotation speed. With the same radiation dose, lower speed results in higher quality four-dimensional images as a result of increased number of projections per phase.

among the images. As shown in Fig. 6, the image acquired with the combination of 1°/s and 10 mA setting had the best quality (smallest RE). For visual comparison, the 1°/s—10 mA and 8°/s—80 mA images are shown in Fig. 7. Moving to slower gantry rotation speed will lead to each phase accumulating more projection data that can be used for reconstruction as compared with faster scans. As a consequence, the integral photon number (filtered back projection) at a spatial point is not reduced in the SGR low-current acquisition as compared with high-current, high-speed scans. Furthermore, at low scan speed, the data become more evenly spared along the 360° circle for each phase, leading to less view-aliasing artifact and consequently to higher image quality.

As shown in Fig. 6, it is found that RE increases almost linearly as a function of the scan speed. Because the total number of projections in a scan, and therefore the number of projections in each phase, varies linearly with the gantry rotation speed, it seems that the RE measure is an appropriate image metric, which has a linear relationship to the number of projections available for generating the phase image.

4D-CBCT imaging with single- and double-gantry rotations

Both SGR and MGR resulted in an increased number of projections. However, as illustrated in Figs. 2b and 2c, the angular distribution of the projections is different for the two acquisition schemes. In general, the efficiency of the MGR method depends on the level of projection redundancy or overlap of the data from the two or more gantry rotations. The 4D-CBCT images acquired with SGR and MGR were compared using the RE metric, and the results are summarized in Fig. 8. Here it is found that for all three motion modes (3.37 s, 4.93 s, and 6.53 s, respectively) and for different combinations of the gantry rotations speed and number of rotations, SGR almost always led to a lower RE or better image quality than the MGR method.

4D-CBCT image quality as a function of the relative speed

The relationship between the image quality and the relative speed is presented in Fig. 9. The data shown in Fig. 9 were fitted with a second order polynomial. The parameters of the model and the goodness of the fit are also shown in the figure. The monotonic dependence of the RE on the relative speed suggests that the relative speed is a meaningful concept in characterizing the 4D-CBCT data acquisition. The quantity "condenses" two important parameters (patient-specific respiration period and the gantry rotation speed) into one and is useful for us to optimize the 4D-CBCT acquisition protocol. In reality, because the respiratory period of a patient can be measured with the aid of a real-time position management signal or similar device (*e.g.*, strain gauge signal) before the 4D-CBCT scanning, a suitable gantry speed can be derived to achieve a prespecified image quality before 4D-CBCT scan. Alternatively, one can use the curve as shown in Fig. 9 to preestimate the 4D image quality for an acquisition setting and to estimate the corresponding patient radiation dose.

DISCUSSION

Cone-beam CT volumetric imaging integrated with a medical linear accelerator opens new avenues for improving current radiation oncology practice. In reality, CBCT has two important applications: patient setup and dose reconstruction/verification. By imaging the patient routinely during a course of radiation therapy, the accuracy of the patient setup can potentially be improved. Furthermore, the CBCT provides a pretreatment patient model on which the dose calculation can be performed using intended fluence maps from the planning system or other means. Both applications rely on the fidelity and quality of the volumetric images. When imaging in the region of thorax and upper abdomen, however, respiration-induced artifacts, such as blurring, doubling, streaking, and distortion are observed, which heavily degrade the image quality, and affect the target

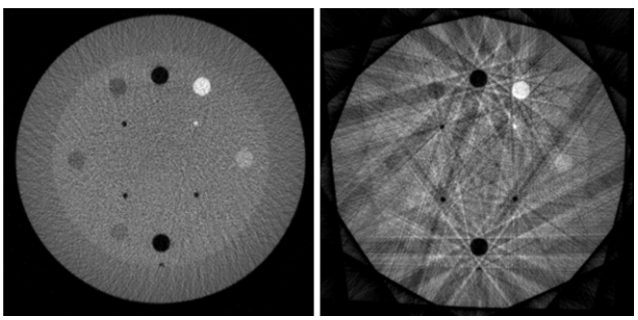

Fig. 7. Comparison of four-dimensional cone-beam computed tomography images acquired with speed 1°/s tube current 10 mA (left) and speed 8°/s tube current 80 mA (right).

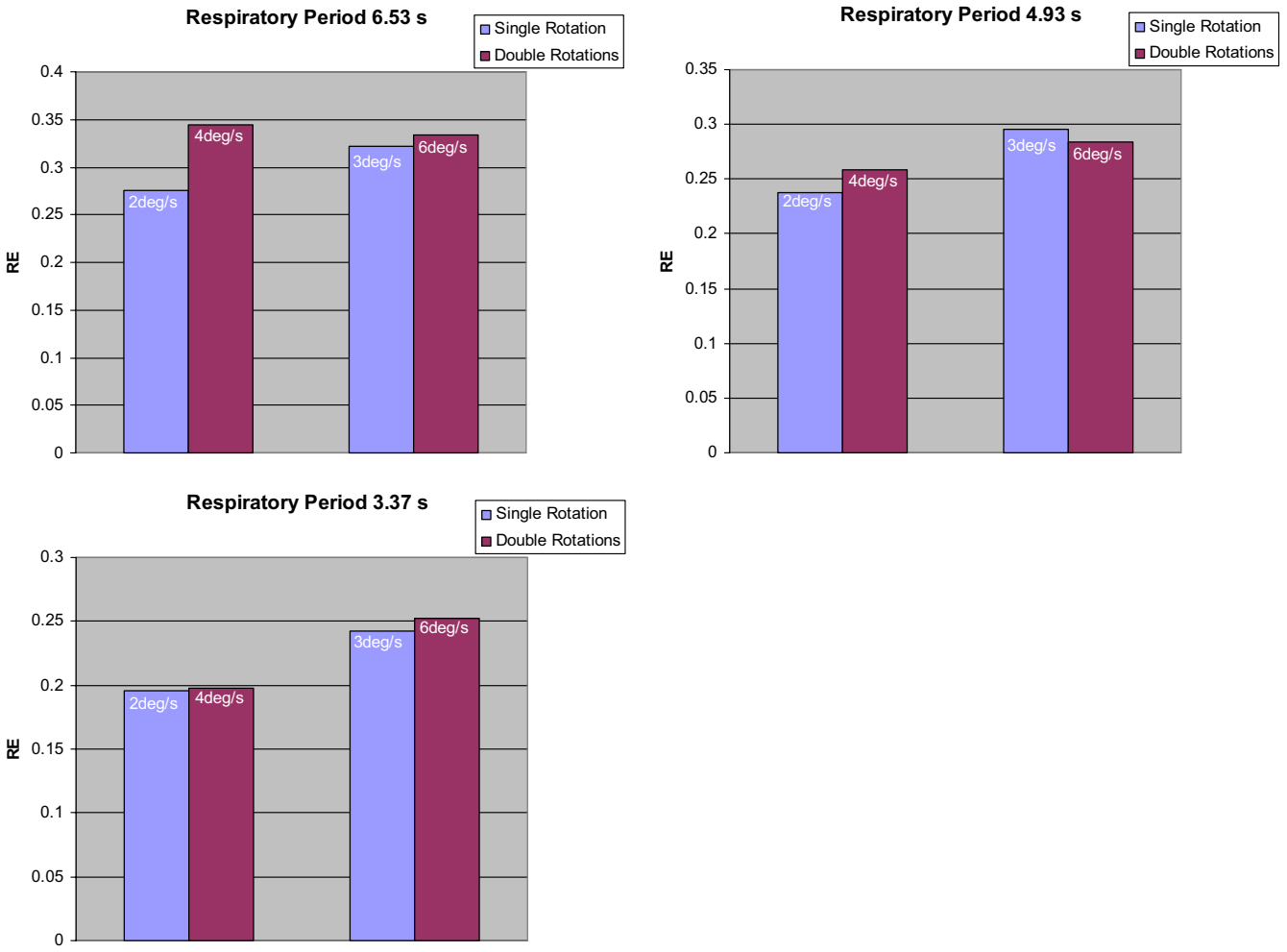

Fig. 8. The effects of increasing the number of rotations and gantry speed. With the same radiation dose, for most of the cases, low rotation speed results in a better image quality than multiple rotations.

localization ability and the accuracy of dose verification. These artifacts in CBCT are much more severe than those found in conventional CT exams because of the relatively slow gantry rotation. In conventional CT, each rotation of the scan can be completed within 0.5 s, during this period the organ/tumor motion is relatively small. Patient body restraints and breath-hold techniques can be used to minimize the motion if necessary. On the contrary, in CBCT scan, the gantry rotation speed is much slower, typically around 1 min for a full 360° scan in acquiring the projection data, which covers more than 10 breathing cycles for most patients. 4D-CBCT or phase-correlated CBCT is an effective way to reduce/eliminate the motion artifacts and makes it useful for guiding the patient setup and dose validation in the presence of organ motion.

Radiation dose is an important issue in CT imaging and, in particular the onboard CBCT imaging because of the repeated use of modality for a given patient. We found that, as we increase the number of projections per phase by slowing down the gantry rotation speed or multiple gantry rotations, the tube current can be lowered accordingly. In this way, the 4D image quality is generally not compromised and one can obtain decent 4D-CT images without increasing the radiation exposure. In a sense, this scheme is to "spread" the photons of a projection in 3D-CBCT to a range of angles in 4D-CBCT imaging, which represents a better tradeoff between the signal-to-noise ratio and the reduction in motion artifacts. In addition to the reduced patient dose, low current is essential to avoid overheating the X-ray tube, especially for an onboard imager without oil cooling system. Although the 4D image quality directly relates to the number of projections available for each phase, there is a limit for slowing down gantry speed. Beyond this limit, the time needed to complete the scan may be too long to cause patient discomfort and extra intrascan motion (other than the respiration-induced motion) may lead to undesirable artifacts. There is a practical need to keep the scanning time as short as possible while maintaining an acceptable image quality. The result shown in Fig. 9 provides guidance for the 4D-CBCT acquisition on a patient-specific basis, which predicts the quality of the 4D images for a certain gantry rotation speed and patient respiratory period. Though patient irregular breathing patterns may alter the number and angular distribution of the pro-

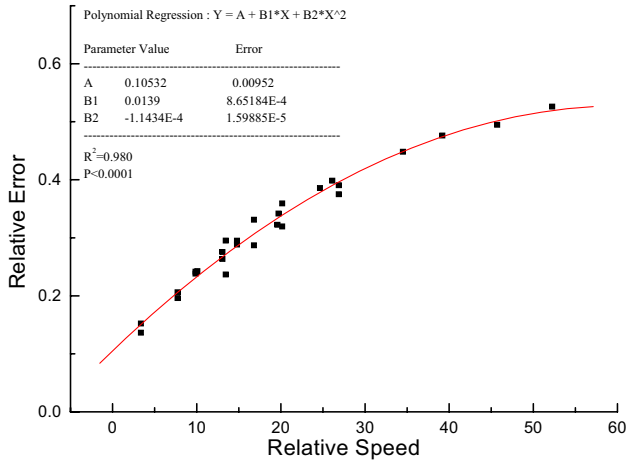

Fig. 9. Relationship between image quality and relative speed of the four-dimensional cone-beam computed tomography scan. The data were acquired for three motion modes with gantry rotation speed varying from 1°/s to 8°/s and constant X-ray tube current (10 mA) and voltage (125 kVp).

jections in each phase and thus change the image qualities, Fig. 9 will nonetheless represent an approximate relation between the image quality and the average patient respiratory period. Obviously, this approximation is valid only when the irregularity of the breathing pattern is not far from ideal periodic motion. It is also worth noting that the influence of breathing irregularity on the 4D images is different from that in conventional fan beam CT, in which the binning artifacts may arise due to mismatch of the slices corresponding to different couch positions.

Although 4D-CBCT technique (SGR or MGR) with phase binning before reconstruction reduces the motion artifacts and improves the image quality, it deals with each phase independently and ignores the correlation of the projections among different phase groups. It is of great interest to reconstruct a 4D object (with spatial and temporal parameters) rather than a series of independent 3D objects (with only spatial parameters), by using simultaneously all the projection data collected in different respiratory phase groups. With the aid of deformable registration and novel reconstruction techniques (9, 22, 27–33), it is possible to incorporate all projection data of different phases into one image reconstruction process. In this way, information from the measurement (CBCT scan) is fully used in the data processing, and more accurate imaging and better dose efficiency may be achieved.

CONCLUSIONS

We have demonstrated that 4D-CBCT images with significantly reduced artifacts can be obtained with a commercially available on-board imager system. A measure of relative error was used to quantify the image quality. At the same radiation dose, the low-current, low-speed acquisition is superior to acquisition with a high current and high speed (<8°/s), and, in most cases, for the same total scanning time, one-rotation low-speed scan is more preferable as compared with an acquisition based on multiple rotations and higher speed. Furthermore, we suggested that 4D-CBCT gantry rotation speed should be determined on a patient-specific basis and have established a quantitative relation between the 4D-CBCT image quality and the relative speed. The approach optimizes the 4D acquisition and makes an efficient use of the available 4D-CBCT technology. The study lays foundation for clinical application of 4D-CBCT and should have significant implication to image-guided radiation therapy.

REFERENCES

1. Xing L, Thorndyke B, Schreibmann E, *et al.* Overview of image-guided radiation therapy. *Med Dosim* 2006;31:91–112.
2. van Herk M, Jaffray D, Betgen A. First clinical experience with cone-beam CT guided radiation therapy: Evaluation of dose and geometric accuracy [Abstract]. *Int J Radiat Oncol Biol Phys* 2004;60(Suppl.):S196.
3. Sidhu K, Ford EC, Spirou S, *et al.* Optimization of conformal thoracic radiotherapy using cone-beam CT imaging for treatment verification. *Int J Radiat Oncol Biol Phys* 2003;55:757–767.
4. Oldham M, Letourneau D, Watt L, *et al.* Cone-beam-CT guided radiation therapy: A model for on-line application. *Radiother Oncol* 2005;75:271–278.
5. Langen KM, Meeks SL, Poole DO, *et al.* The use of megavoltage CT (MVCT) images for dose recomputations. *Phys Med Biol* 2005;50:4259–4276.
6. Mohan R, Zhang X, Wang H, *et al.* Use of deformed intensity distributions for on-line modification of image-guided IMRT to account for interfractional anatomic changes. *Int J Radiat Oncol Biol Phys* 2005;61:1258–1266.
7. Wu Q, Liang J, Yan D. Application of dose compensation in image-guided radiotherapy of prostate cancer. *Phys Med Biol* 2006;51:1405–1419.
8. Jaffray DA, Siewerdsen JH, Wong JW, *et al.* Flat-panel cone-beam computed tomography for image-guided radiation therapy. *Int J Radiat Oncol Biol Phys* 2002;53:1337–1349.
9. Yang Y, Schreibmann E, Li T, Xing L. Motion correction for improved target localization with on-board cone-beam computed tomography. *Phys Med Biol* 2006;51:253–267.
10. Li T, Schreibmann E, Yang Y, Xing L. Dosimetric evaluation of kV cone-beam CT (CBCT) based dose calculation. *Phys Med Biol.* In press.
11. Lo T, Yang Y, Schreibmann E, *et al.* Mapping electron density distribution from planning CT to cone-beam CT (CBCT): A novel strategy for accurate dose calculation based on CBCT. *Int J Radiat Oncol Biol Phys* 2005;63(Suppl. 2):S507.
12. Letourneau D, Martinez AA, Lockman D, *et al.* Assessment of residual error for online cone-beam CT-guided treatment of prostate cancer patients. *Int J Radiat Oncol Biol Phys* 2005;62:1239–1246.
13. Sonke JJ, Zijp L, Remeijer P, *et al.* Respiratory correlated cone beam CT. *Med Phys* 2005;32:1176–1186.
14. Moseley DJ, Hawkins M, Eccles C, *et al.* Respiratory gated cone-beam CT volumetric imaging for external beam radiotherapy. *Int J Radiat Oncol Biol Phys* 2005;63(Suppl. 1):s27–s28.
15. Sonke JJ, Van Herk M, Belderbos J, *et al.* An off-line 4D cone

ARTICLE IN PRESS

beam CT based correction protocol for lung tumor motion. *Int J Radiat Oncol Biol Phys* 2005;63(Suppl. 1):s389–s390.
16. Crowther RA, DeRosier DJ, Kug A. The reconstruction of a three-dimensional structure from projections and its application to electron microscopy. *Proc R Soc London Ser A* 1970; 317:319–340.
17. Low DA, Nystrom M, Kalinin E, *et al.* A method for the reconstruction of four-dimensional synchronized CT scans acquired during free breathing. *Med Phys* 2003;30:1254–1263.
18. Rietzel E, Chen GTY. Improving retrospective sorting of 4D computed tomography data. *Med Phys* 2006;33:377–379.
19. Rietzel E, Pan T, Chen GTY. Four-dimensional computed tomography: Image formation and clinical protocol. *Med Phys* 2005;32:874–889.
20. Pan T, Lee TY, Rietzel E, *et al.* 4D-CT imaging of a volume influenced by respiratory motion on multi-slice CT. *Med Phys* 2004;31:333–340.
21. Vedam SS, Keall PJ, Kini VR, *et al.* Acquiring a four-dimensional computed tomography dataset using an external respiratory signal. *Phys Med Biol* 2003;48:45–62.
22. Li T, Schreibmann E, Thorndyke B, *et al.* Radiation dose reduction in four-dimensional computed tomography. *Med Phys* 2005;32:3650–3660.
23. Pan T. Comparison of helical and cine acquisitions for 4D-CT imaging with multislice CT. *Med Phys* 2005;32:627–634.
24. Wink N, Panknin C, Solberg TD. Phase versus amplitude sorting of 4D-CT data. *J Appl Clin Med Phys* 2006;7:77–85.
25. Wink NM, McNitt-Gray MF, Solberg TD. Optimization of multi-slice helical respiration-correlated CT: The effects of table speed and rotation time. *Phys Med Biol* 2005;50:5717–5729.
26. Li T, Xing L, Munro P, *et al.* 4D cone-beam CT (CBCT) using an on-board imager. *Med Phys* 2006;33:3825–3833.
27. Li T, Thorndyke B, Schreibmann E, Xing L. Model-based image reconstruction for four-dimensional PET. *Med Phys* 2006;33:1288–1298.
28. Schreibmann E, Chen GT, Xing L. Image interpolation in 4D CT using a BSpline deformable registration model. *Int J Radiat Oncol Biol Phys* 2006;64:1537–1550.
29. Zeng R, Fessler JA, Balter JM. Respiratory motion estimation from slowly rotating x-ray projections: Theory and simulation. *Med Phys* 2005;32:984–991.
30. Coselmon MM, Balter JM, McShan DL, *et al.* Mutual information based CT registration of the lung at exhale and inhale breathing states using thin-plate splines. *Med Phys* 2004;31:2942–2948.
31. Brock KM, Balter JM, Dawson LA, *et al.* Automated generation of a four-dimensional model of the liver using warping and mutual information. *Med Phys* 2003;30:1128–1133.
32. Zou Y, Sidky EY, Pan X. Partial volume and aliasing artefacts in helical cone-beam CT. *Phys Med Biol* 2004;49:2365–2375.
33. Zou Y, Pan X. Exact image reconstruction on PI-lines from minimum data in helical cone-beam CT. *Phys Med Biol* 2004; 49:941–959.

Enhanced 4D Cone-Beam CT with Inter-Phase Motion Model

Tianfang Li, Albert Koong, and Lei Xing[a]

Department of Radiation Oncology, Stanford University School of Medicine

Stanford, CA 94305

Short title: Enhanced 4D CBCT

[a)] Author to whom correspondence should be addressed:

Department of Radiation Oncology
Stanford University School of Medicine,
Clinical Cancer Center
875 Blake Wilbur Drive, Rm CC-G204
Stanford, CA 94305-5847
Telephone: (650) 498-7896
Fax: (650) 498-4015
Email: lei@reyes.stanford.edu

Submitted to: *Medical Physics*

Abstract

Four-dimensional (4D) cone-beam CT (CBCT) is commonly obtained by respiratory phase binning of the projections, followed by independent reconstructions of the rebinned data in each phase bin. Due to the significantly reduced number of projections per reconstruction, the quality of the 4DCBCT images is often degraded by view-aliasing artifacts seen in the axial view. Acquisitions using multiple gantry rotations or slow gantry rotation can increase the number of projections and substantially improve the 4D images. However, the extra cost of the scan time may set fundamental limits of their applications in clinics. Improving the trade-off between image quality and scan time is the key to making 4D onboard imaging practical and more useful. In this paper, we present a novel technique toward high-quality 4DCBCT imaging without prolonging the acquisition time, referred to as the "enhanced 4DCBCT". The method correlates the data in different phase bins and integrates the internal motion into the 4DCBCT image formulation. Several strategies of the motion derivation are discussed, and the resultant images are assessed with numerical simulations as well as a clinical case.

.

Key words: cone-beam, 4D CT, on-board imager, IGRT, organ motion

I. Introduction

Medical linear accelerators equipped with cone-beam CT (CBCT) imaging system, using either kV or MV x-ray source, have recently become available in clinics. The volumetric image provided by CBCT opens new avenues for patient setup, dose verification, and online treatment planning [1-12]. These applications rely highly upon the fidelity and quality of the CBCT images. When imaging in the region of thorax and upper abdomen, however, respiration induced artifacts, such as blurring, doubling, streaking and distortion are observed, which heavily degrade the image quality, and affect the target localization ability and the accuracy of dose calculation [13,14].

A recently proposed method to account for respiratory motion during CBCT imaging is called "respiration correlated CBCT" or four-dimensional (4D) CBCT [15-18] . In this method, the CBCT projections are divided into several groups as according to their respiratory phases. Each phase group is then reconstructed independently to yield a volumetric image corresponding to that specific phase. Since the selected projections in each group have almost the same phase, the method greatly reduces the motion-induced inconsistency among the data, leading to improved image reconstruction. However, the number of projections available for each image reconstruction is substantially decreased compared to a conventional 3D CBCT due to the data dividing. This may lead to serious undersampling problem and result in strong view-aliasing artifacts in the phase-resolved images. The artifacts are generated during the backprojection step in the CBCT image reconstruction process and are mainly seen in the 2D axial planes.

To eliminate the view-aliasing artifacts in 4DCBCT, we have recently investigated acquisition techniques of "multiple gantry rotation" and "slow gantry rotation" with low x-ray tube current [16,17]. These methods increase the number of projections of each phase and significantly improve the 4DCBCT image quality. However a practical issue is the prolonged acquisition time, which may limit their clinical applications.

The purpose of this work is to investigate a novel approach to reduce the acquisition time while maintaining the 4DCBCT image quality, or from another point of view, to enhance the current 4DCBCT image quality while using short acquisition time.

The approach developed in this paper is essentially to reduce the view-aliasing artifacts resulted from insufficient sampling. To increase the sampling rate in each individual phase, projections of all other phases can be incorporated into the reconstruction process. To do so, a motion model linking the data of different phases is required, which can be derived from deformable registrations of the 4DCBCT phases. Two other registration strategies of introducing an additional diagnostic CT image and mapping between image space and projection space are also investigated. The proposed approach is evaluated with numerical simulations. Since the view-aliasing artifacts are prominent only in the axial view and for simplicity, we start with fan-beam (2D) geometry to study the performance of the approach, a clinical case of a lung cancer patient is then presented.

II. Methods and Materials

A. Reconstruction for reduced view-aliasing artifacts

As described earlier, to form the 4DCBCT images, the acquired projection data are retrospectively sorted into several phase bins before reconstructions. When the acquisition time is limited, the reduced number of projections per reconstruction will result in undersampling and degrade the image with view-aliasing artifacts. In order to improve the sampling rate in each phase, we need to borrow projection information from other phases. Obviously, direct inclusion of projections of other phases will cause the inconsistency in the data due to the patient motion. However, as we have shown previously, if the motion can be accurately modeled, a motion-corrected CBCT reconstruction can be obtained [19]. The idea is to perform the backprojections of the filtered data along deformed paths according to the corresponding motion. Equivalently and computationally more efficiently, one can reconstruct each individual phase first, then superimpose all the phases after deforming each of them into the same phase based on the given motion model. In the next, we focus on discussing different ways to deriving the motion model.

B. Motion model estimation

A1. Register artifacts-contaminated 4D images

The most straightforward way to find the motion model is to register the 4DCBCT phases using a deformable model. A unique problem here is that the images to be registered contain serious steak artifacts, which may adversely affect the accuracy of the derived motion model, and the error can propagate into the final 4DCBCT images. Nevertheless, the process may prove to be favorable because of greatly reduced view-aliasing artifacts. The performance of this method is shown later with a simulation study, where the registration was done based on a free-form Spline (BSpline) model. The simplicity and yet accuracy of the BSpline method make it a preferred tool for many clinical applications [20-24]. More details about this registration algorithm can be found in Ref. [22].

A2. Register planning CT to 4DCBCT phased image

Note that in radiation therapy, it is often the case that a patient has already got a 3D or 4D CT scan for the treatment planning prior to any radiation delivery. In such case, an artifact-free volumetric image can be assumed available upon the 4DCBCT scan. The idea is to match this artifact-free 3D image with each phase of the 4DCBCT images to derive the motion model. Since only one of the two images being registered has artifacts, it is expected that the accuracy will be improved over the first procedure. Again, the performance of this method is evaluated with the simulation study later in this paper.

A3. Registration from image space to projection space

Although the reconstructed 4DCBCT phase images contain view-aliasing artifacts, one should realize that the artifacts are not originally present in the raw data but are generated later during the reconstruction process. Therefore, we may avoid the drawback of using low-quality reconstructed image in deriving the motion model by registering the 3D planning CT directly to the CBCT raw data (after phase sorting). Note the two images being registered are in different spaces, in the following, we present a simple algorithm for such a registration task using a BSpline model.

Similar to the conventional image registration using deformable models, the motion of the object is described by $g(\boldsymbol{x};t) = f(\boldsymbol{x} + \boldsymbol{u}(\boldsymbol{x};t))$, where $f(\boldsymbol{x})$ represents the

3D image obtained from the planning CT scan, $g(\boldsymbol{x};t)$ is the same object at a particular phase t during the 4DCBCT scan, and $\boldsymbol{u}(\boldsymbol{x};t)$ defines the corresponding deformation for point $\boldsymbol{x}$ at that phase. With the BSpline model, the deformation is defined on a sparse, regular grid of control points λ_n placed over the CT image. When a point is not on the grid, the associated deformation is calculated by the B-spline interpolation as follows

$$\boldsymbol{u}(\boldsymbol{x};t) = \sum_n \theta_{n,t}\beta^{(3)}(\frac{\boldsymbol{x}-\lambda_n}{\Delta_x}), \quad (1)$$

where $\beta^{(3)}(\boldsymbol{x}) = \beta^{(3)}(x)\beta^{(3)}(y)\beta^{(3)}(z)$ is a separable cubic B-spline convolution kernel, $\theta_{n,t}$ are the values for the control points at phase t, and Δ_x controls the grid spacing in each dimension.

To register the CBCT projections with the planning CT image, we adopt the metric of sum of squared difference,

$$\Phi(\boldsymbol{\theta}) = \sum_i (Y_i - \sum_j A_{ij} g_j)^2 = \sum_i (Y_i - \sum_j A_{ij} f_j(\boldsymbol{x}+\boldsymbol{u}))^2, \quad (2)$$

where Y_i is the total attenuation along the ith projection ray, j is the index of the image voxel, and A is the cone-beam projection matrix. For simplicity, the phase index t is neglected here. Given the projection data Y and planning CT image f, the deformation field $\boldsymbol{u}$ at a particular phase can be found by minimizing the above objective function. General-purpose algorithms can be applied to solve the optimization problem, and in this work the LBFSG algorithm is used [25], which requires the calculation of the first derivative of the cost function Φ. It can be shown that (2) has a closed-form derivative that can be calculated explicitly. For a similar derivation, readers are referred to the appendix of [26].

C. Simulation study

While the above developed appoach intended for 3D cone-beam geomery, we found it convenient to demonstrate the performances of the different algorithms in 2D fan-beam geometry. The parameters for the 2D numerical simulations were similar to the real setup of a Varian Trilogy machine (Varian Medical Systems, Palo Alto, CA), where the focal length of the fan beam was 150 cm and the radius of the detector rotation was

50 cm. The fan beam had 1024 samples spaced by 0.388 mm, and 2048 projection views were simulated with projection angles evenly spanned over 360^{o}. The object used in the simulations came from one slice of the CT images of a patient, which contained 512x512 pixels with the pixel size of 1.0 mm. To include the effect of the respiratory-induced motion, we imposed an arbitrary perodically changing deformation field on the image during the CT simulation, with the maximum motion applitude of approximately 3 cm and the period of 4 second. In reality, irregular patient respiration is possible, which may affect the accuracy of phase binning in 4DCBCT. However, this was not considered in our simulations because the focus of this paper is the reduction of the view-aliasing artifacts.

D. Patient study

A lung cancer patient had a multiple-gantry-rotation (MGR) 4DCBCT scan in our clinic and his 4D images were used to evaluate our proposed approach. Due to the limit access of the available data, only the method described in section A1 was tested. The 4DCBCT was acquired with a Trilogy system (Varian Medical Systems, Palo Alto, CA). For the MGR 4D scan, the x-ray tube current was set to 32 mA, and four gantry rotations were performed at a speed of 6^{o}/s. Each rotation (slightly over 360 deg) consisted of over 680 projections, and the effective area of each acquired projection image was 397.312 mm x 297.984 mm, containing 1024x768 pixels. The average breathing cycle of the patient was 4.2 sec. The 4DCBCT images were obtained by retrospective sorting of the MGR data into 6 phases and subsequently reconstructing the rebinned data. More details about this 4DCBCT technique can be found in [16]. To evaluate the proposed 4D image enhancing method, the 4D phases were registered to the 0% phase with BSpline deformable model and then superimposed. The resultant phase-0% image was then compared with the original 4DCBCT for several axial slices to demonstrate the differences.

III. Results

A. Simulation study

The simulated projection data are shown in Figs. 1a and 1b, where the left is from the static CT image and the right is from the same object with the artificial in-plane deformation. It is seen that the object motion during the scan generated large amount of inconsistency in the projection data (Fig. 1b). To show its effect on the resultant image, in Fig. 1c and 1d, the corresponding reconstructed images are compared, where artifacts such as blurring, doubling, distortion, and streak artifacts are observed in the motion contaminated image (Fig. 1d).

The simulated projections of the continuously deformed image were retrospectively sorted into 8 phases. Five of the reconstructed phases from the peak inspiration to the peak expiration are illustrated in Fig. 2a, and a zoomed-in image of the phase 1 is shown in Fig. 2b. Compared with the reconstructed images in Fig. 1c and 1d, it can be found that the motion blurring is greatly reduced and the boundary of the primary tumor became much clearer after the phase sorting. However, some low contrast structures (for example the aorta, muscle, etc) are lost due to the view-aliasing streak artifacts.

Three enhanced images using the proposed approach are shown in Fig. 3 corresponding to the three motion model derivation techniques. The top row in Fig. 3 shows the derived deformation between phase 1 and phase 4, where from the left to the right are using “4D phase-to-phase registration” (method A1), “CT image to 4D phases” (method A2), and “CT image to CBCT projection” (method A3), respectively. The corresponding reconstructed images (at phase 1) are shown in the middle row, and the difference images (by subtracting the true CT image) are shown in the bottom. From these images, we found that the image enhancing approach using any of the three motion model improved the image quality over the regular phase-resolved image, and the method as described in section A3 by matching CT image with CBCT raw data generated the best final images, because a relatively more accurate motion model is applied.

A. Patient study

The enhanced 4DCBCT images were obtained for the patient using the proposed approach and the motion model derived with method A1. In Fig 4. the resultant image

phase 1 is shown along with the image of the same phase before the enhancement. Though the artifacts in the original 4D images are not prominent, it is found the proposed technique improved the image quality and more details are revealed after the process.

IV. Discussion and Conclusion

One goal of 4DCBCT is to remove the respiratory motion induced artifacts in the reconstructed images to increase the accuracy of target localization and dose calculation. Different from conventional 4DCT [27-29], 4DCBCT acquisition with an onboard imager usually has a much slower speed about 1 min per rotation, and due to the limited total scan time in practice, undersampling is often an issue resulting in severely degraded 4D images, which sometimes are even worse than the motion contaminated 3D images. The approach proposed in this paper reconstructs the image of any particular phase by introducing additional information from other phases, effectively increasing the sampling rate and improving the image quality. In general, the approach relies on the accuracy of the motion model that relates different projections. We have demonstrated with 2D simulations that the best way to derive the motion model is to register the artifact-free CT images with the CBCT projections, if a planning CT scan has been performed prior to the CBCT scan. Though the registration accuracy in 3D geometry may be different from 2D geometry, these basic principles and relative performances observed in this paper are expected true. As an example, the real patient case shown in this paper demonstrated the feasibility of the proposed method under the worst condition (low view-aliasing artifacts in the 4D images leaves little space for further improvement, low accuracy in motion derivation by using method A1 limits the performance of the proposed approach).

As it is known, the radiation dose has been one of the major concerns in CBCT imaging because of the repeated use for a given patient. With the proposed approach, it is possible to lower the x-ray tube current hence the radiation exposure for the 4DCBCT scan while maintaining a meaningful 4D image, because introducing additional information of other phases during reconstruction effectively increases the photon statistics. This is similar to the case of 4D fan-beam CT studied earlier by our group [30].

The efficacy of the approach in improving the tradeoff between the controlled radiation exposure and the resultant CBCT image quality is being investigated.

It should be noted that the proposed 4DCBCT enhancing technique needs computation of the deformation field before the image reconstruction, which takes extra time compared to regular CBCT imaging. Currently, a 3D image-to-image registration with image size of 512x512x64 will take approximately 30 minutes. The image-to-projection registration method generally takes longer because of the calculation of the forward projections. The computational time makes it difficult for online applications in the treatment room. However, development of techniques in speeding up the algorithms as well as the computer hardware is highly promising, which we believe will make the 4DCBCT imaging fast and reliable in the near future. In addition, the 4DCBCT image quality may be further improved by advanced reconstruction algorithm and helical scan mode [31-33].

In conclusion, we have developed a novel approach to enhance the 4DCBCT image quality. The enhancement is achieved by increasing the angular sampling rate of each phase of the 4DCBCT data using information from other phases, thus the view-aliasing artifacts commonly seen in the limited-time scan 4DCBCT images are eliminated or significantly reduced. The approach opens new opportunities for 4DCBCT to be a more useful tool that may substantially improve the current cancer management in radiation oncology.

Acknowledgement

This work was supported in part by grants from the Department of Defense (W81XWH-0610235) and Susan Komen Breast Cancer Foundation.

Reference:

[1] L. Xing, B. Thorndyke, E. Schreibmann, Y. Yang, T. F. Li, G. Y. Kim, G. Luxton, and A. Koong, "Overview of image-guided radiation therapy," Med Dosim **31**(2)**,** 91-112 (2006).

[2] R. I. Berbeco, S. B. Jiang, G. C. Sharp, G. T. Chen, H. Mostafavi, and H. Shirato, "Integrated radiotherapy imaging system (IRIS): design considerations of tumour tracking with linac gantry-mounted diagnostic x-ray systems with flat-panel detectors," Phys Med Biol **49**(2)**,** 243-55 (2004).

[3] M. J. Ghilezan, D. A. Jaffray, J. H. Siewerdsen, M. Van Herk, A. Shetty, M. B. Sharpe, S. Zafar Jafri, F. A. Vicini, R. C. Matter, D. S. Brabbins, and A. A. Martinez, "Prostate gland motion assessed with cine-magnetic resonance imaging (cine-MRI)," Int J Radiat Oncol Biol Phys **62**(2)**,** 406-17 (2005).

[4] D. Letourneau, A. A. Martinez, D. Lockman, D. Yan, C. Vargas, G. Ivaldi, and J. Wong, "Assessment of residual error for online cone-beam CT-guided treatment of prostate cancer patients," Int J Radiat Oncol Biol Phys **62**(4)**,** 1239-46 (2005).

[5] T. R. Mackie, J. Kapatoes, K. Ruchala, W. Lu, C. Wu, G. Olivera, L. Forrest, W. Tome, J. Welsh, R. Jeraj, P. Harari, P. Reckwerdt, B. Paliwal, M. Ritter, H. Keller, J. Fowler, and M. Mehta, "Image guidance for precise conformal radiotherapy," Int J Radiat Oncol Biol Phys **56**(1)**,** 89-105 (2003).

[6] R. Mohan, X. Zhang, H. Wang, Y. Kang, X. Wang, H. Liu, K. K. Ang, D. Kuban, and L. Dong, "Use of deformed intensity distributions for on-line modification of image-guided IMRT to account for interfractional anatomic changes," Int J Radiat Oncol Biol Phys **61**(4)**,** 1258-66 (2005).

[7] H. Shirato, S. Shimizu, T. Kunieda, K. Kitamura, M. van Herk, K. Kagei, T. Nishioka, S. Hashimoto, K. Fujita, H. Aoyama, K. Tsuchiya, K. Kudo, and K. Miyasaka, "Physical aspects of a real-time tumor-tracking system for gated radiotherapy," Int J Radiat Oncol Biol Phys **48**(4)**,** 1187-95 (2000).

[8] S. L. Meeks, J. F. Harmon, Jr., K. M. Langen, T. R. Willoughby, T. H. Wagner, and P. A. Kupelian, "Performance characterization of megavoltage computed tomography imaging on a helical tomotherapy unit," Med Phys **32**(8)**,** 2673-81 (2005).

[9] J. Pouliot, A. Bani-Hashemi, J. Chen, M. Svatos, F. Ghelmansarai, M. Mitschke, M. Aubin, P. Xia, O. Morin, K. Bucci, M. Roach, 3rd, P. Hernandez, Z. Zheng, D. Hristov, and L. Verhey, "Low-dose megavoltage cone-beam CT for radiation therapy," Int J Radiat Oncol Biol Phys **61**(2)**,** 552-60 (2005).

[10] K. M. Langen, S. L. Meeks, D. O. Poole, T. H. Wagner, T. R. Willoughby, P. A. Kupelian, K. J. Ruchala, J. Haimerl, and G. H. Olivera, "The use of megavoltage CT (MVCT) images for dose recomputations," Phys Med Biol **50**(18)**,** 4259-76 (2005).

[11] C. F. Elder, W. K. Rebecca, D. Letourneau, D. A. Jaffray, J. Bissonnette, A. Bezjak, P. Greg, W. Elizabeth, M. Carol, M. Michael, S. Michael, and G. Mary, "Towards a one-step scan and treat process for palliative radiotherapy - a potential application for cone beam computerized tomography (CBCT)," Int J Radiat Oncol Biol Phys **63**(2, Supplement)**,** S440 (2005).

[12] M. Oldham, D. Letourneau, L. Watt, G. Hugo, D. Yan, D. Lockman, L. H. Kim, P. Y. Chen, A. Martinez, and J. W. Wong, "Cone-beam-CT guided radiation therapy: A model for on-line application," Radiother Oncol **75**(3)**,** 271-8 (2005).

[13] Y. Yang, E. Schreibmann, T. Li, C. King, and L. Xing, "Dosimetric evaluation of kV cone-beam CT (CBCT) based dose calculation," Phys Med Biol**,** Submitted (2006).

[14] T. Lo, Y. Yang, E. Schreibmann, T. Li, and L. Xing, "Mapping electron density distribution from planning CT to cone-beam CT (CBCT): a novel strategy for accurate dose calculation based on CBCT," Int J Radiat Oncol Biol Phys **63**(2, Supplement)**,** S507 (2005).

[15] J. J. Sonke, L. Zijp, P. Remeijer, and M. van Herk, "Respiratory correlated cone beam CT," Med Phys **32**(4)**,** 1176-86 (2005).

[16] T. Li, L. Xing, P. Munro, C. McGuinness, M. Chao, Y. Yang, B. Loo, and A. Koong, "Four-dimensional cone-beam computed tomography using an on-board imager," Medical Physics **33**(10)**,** 3825-3833 (2006).

[17] T. Li and L. Xing, "Optimize 4D cone-beam CT acquisition protocol for external beam radiotherapy," Int J Radiat Oncol Biol Phys **in press** (2006).

[18] L. Dietrich, S. Jetter, T. Tucking, S. Nill, and U. Oelfke, "Linac-integrated 4D cone beam CT: first experimental results," Phys Med Biol **51**(11)**,** 2939-52 (2006).

[19] T. Li, E. Schreibmann, Y. Yang, and L. Xing, "Motion correction for improved target localization with on-board cone-beam computed tomography," Phys Med Biol **51**(2)**,** 253-67 (2006).

[20] D. Mattes, D. R. Haynor, H. Vesselle, T. K. Lewellen, and W. Eubank, "PET-CT image registration in the chest using free-form deformations," IEEE Trans Med Imaging **22**(1)**,** 120-8 (2003).

[21] T. Rohlfing, C. R. Maurer, Jr., D. A. Bluemke, and M. A. Jacobs, "Volume-preserving nonrigid registration of MR breast images using free-form deformation with an incompressibility constraint," IEEE Trans Med Imaging **22**(6)**,** 730-41 (2003).

[22] D. Rueckert, L. I. Sonoda, C. Hayes, D. L. Hill, M. O. Leach, and D. J. Hawkes, "Nonrigid registration using free-form deformations: application to breast MR images," IEEE Trans Med Imaging **18**(8)**,** 712-21 (1999).

[23] E. Schreibmann, G. T. Chen, and L. Xing, "Image interpolation in 4D CT using a BSpline deformable registration model," Int J Radiat Oncol Biol Phys **64**(5)**,** 1537-50 (2006).

[24] J. W. Wolthaus, M. van Herk, S. H. Muller, J. S. Belderbos, J. V. Lebesque, J. A. de Bois, M. M. Rossi, and E. M. Damen, "Fusion of respiration-correlated PET and CT scans: correlated lung tumour motion in anatomical and functional scans," Phys Med Biol **50**(7)**,** 1569-83 (2005).

[25] D. C. Liu and J. Nocedal, "On the limited memory BFGS method for large scale optimization," Mathematical Programming **45,** 503-528 (1989).

[26] R. Zeng, J. A. Fessler, and J. M. Balter, "Respiratory motion estimation from slowly rotating x-ray projections: theory and simulation," Med Phys **32**(4)**,** 984-91 (2005).

[27] T. Pan, "Comparison of helical and cine acquisitions for 4D-CT imaging with multislice CT," Med Phys **32**(2)**,** 627-34 (2005).

[28] T. Pan, T. Y. Lee, E. Rietzel, and G. T. Chen, "4D-CT imaging of a volume influenced by respiratory motion on multi-slice CT," Med Phys **31**(2)**,** 333-40 (2004).

[29] S. S. Vedam, P. J. Keall, V. R. Kini, H. Mostafavi, H. P. Shukla, and R. Mohan, "Acquiring a four-dimensional computed tomography dataset using an external respiratory signal," Phys Med Biol **48**(1)**,** 45-62 (2003).

[30] T. Li, E. Schreibmann, B. Thorndyke, G. Tillman, A. Boyer, A. Koong, K. Goodman, and L. Xing, "Radiation dose reduction in four-dimensional computed tomography," Med Phys **32**(12)**,** 3650-60 (2005).

[31] X. Pan, Y. Zou, and D. Xia, "Image reconstruction in peripheral and central regions-of-interest and data redundancy," Med Phys **32**(3)**,** 673-84 (2005).

[32] X. Pan, Y. Zou, D. Xia, and E. Y. Sidky, "Reconstruction of 3D regions-of-interest from data in reduced helical cone-beam scans," Technol Cancer Res Treat **4**(2)**,** 143-50 (2005).

[33] Y. Zou, E. Y. Sidky, and X. Pan, "Partial volume and aliasing artefacts in helical cone-beam CT," Phys Med Biol **49**(11)**,** 2365-75 (2004).

Figure Captions

Figure 1. Simulated projections and their corresponding reconstructed images. The left column is from the static object and the right column is from the same object with artificial deformation.

Figure 2. (a) Five examples of the reconstructed phases after the phase sorting of the simulated projection data of the moving object; (b) a zoomed-in image of the first reconstructed phase, where it is found that the motion blurring is reduced by phase binning, but some low-contrast structures are lost due to view-aliasing artifacts.

Figure 3. The first row, from the left to the right, illustrates the difference of the derived deformation field obtained by methods A1, A2 and A3, respectively. The second row shows the corresponding reconstructed images for phase 1 using the proposed image enhancement technique. The third low is the difference images obtained by subtracting from the second row the true image (*i.e.* conventional reconstruction of a static object).

Figure 4. 4DCBCT images of a patient. The left column shows three arbitrary slices of the peak inspiration phase, and the right column is the corresponding images after the proposed enhancement with motion model derived by using method A1.

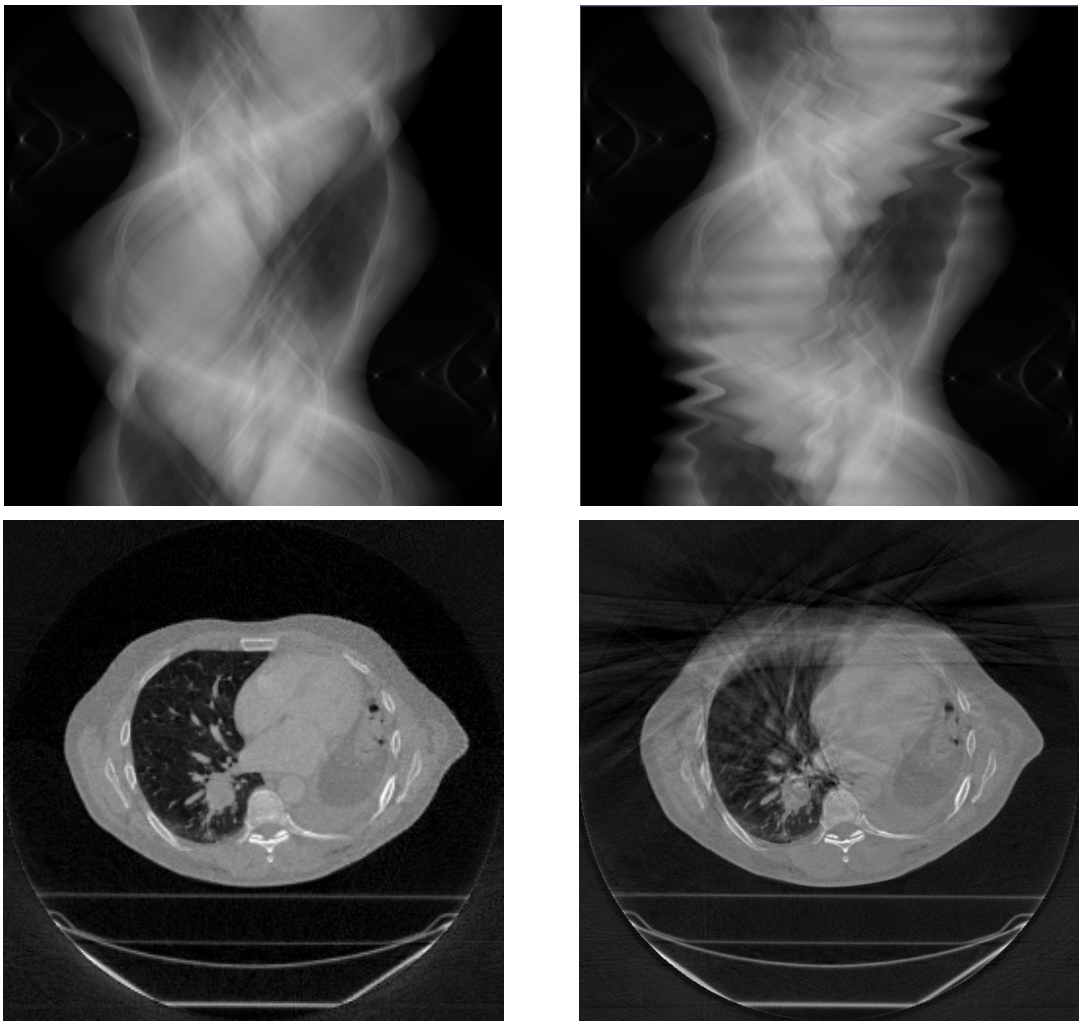

Figure 1

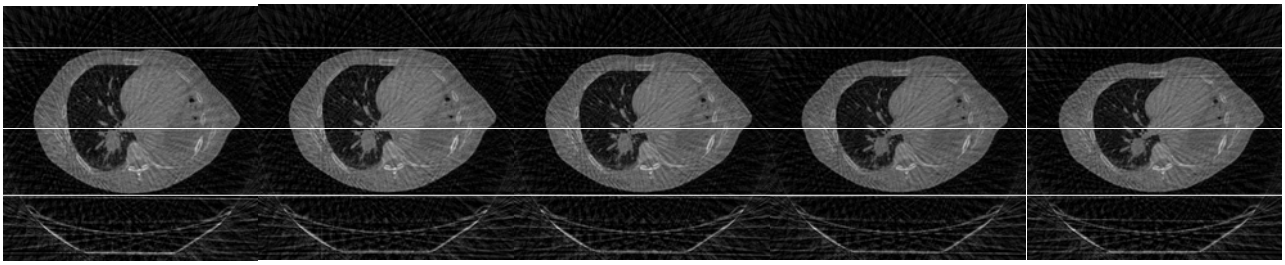

(a)

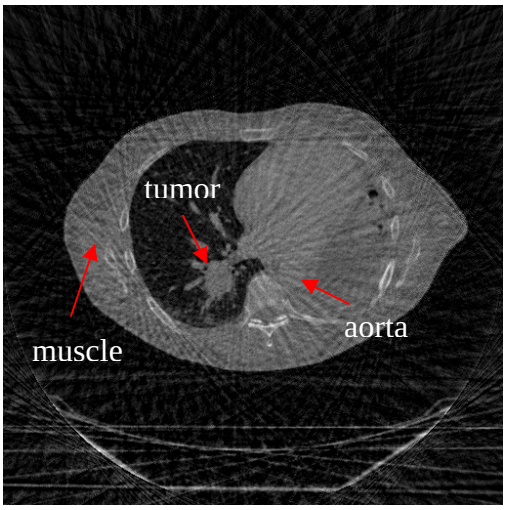

(b)

Figure 2.

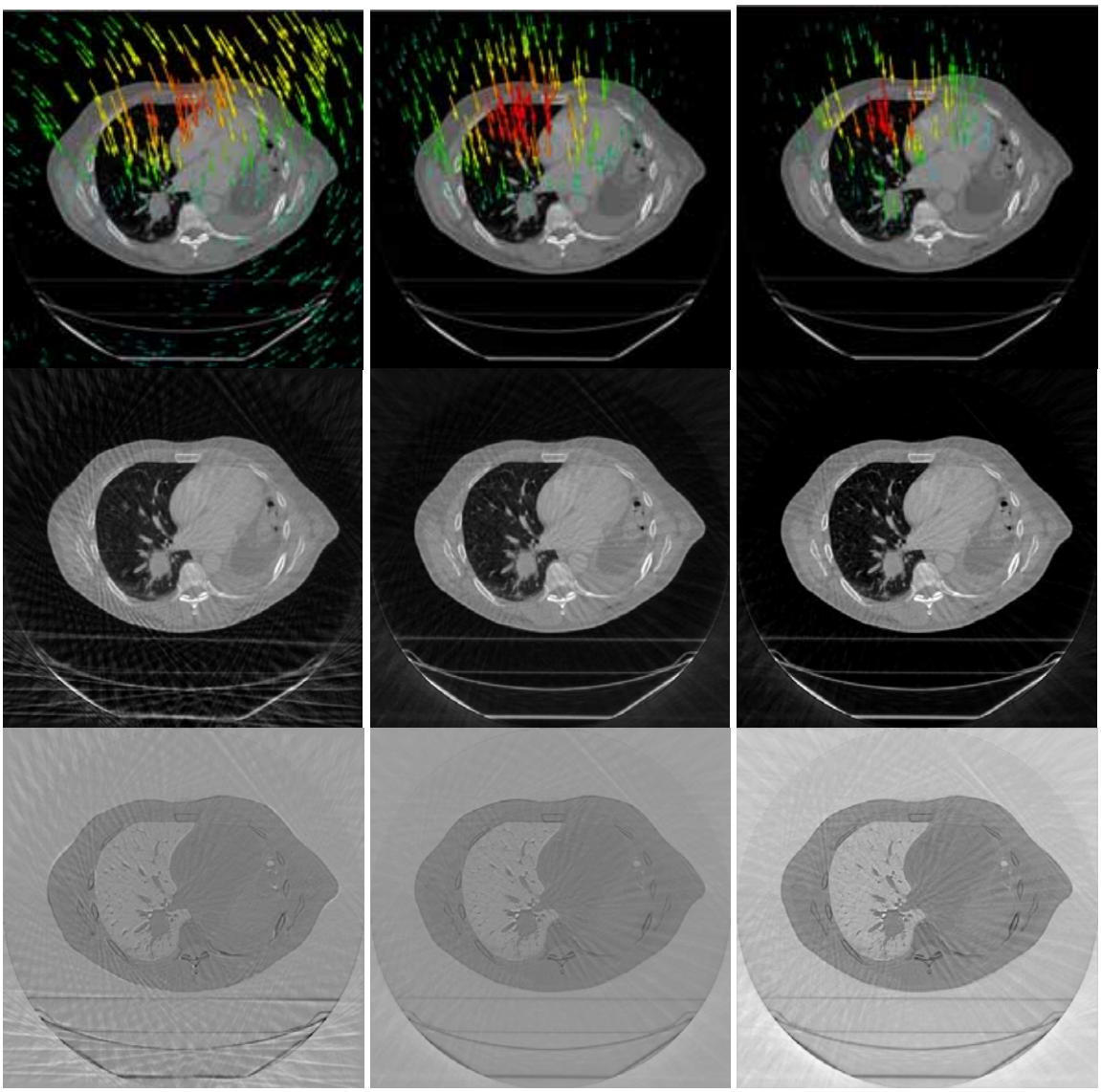

Figure 3.

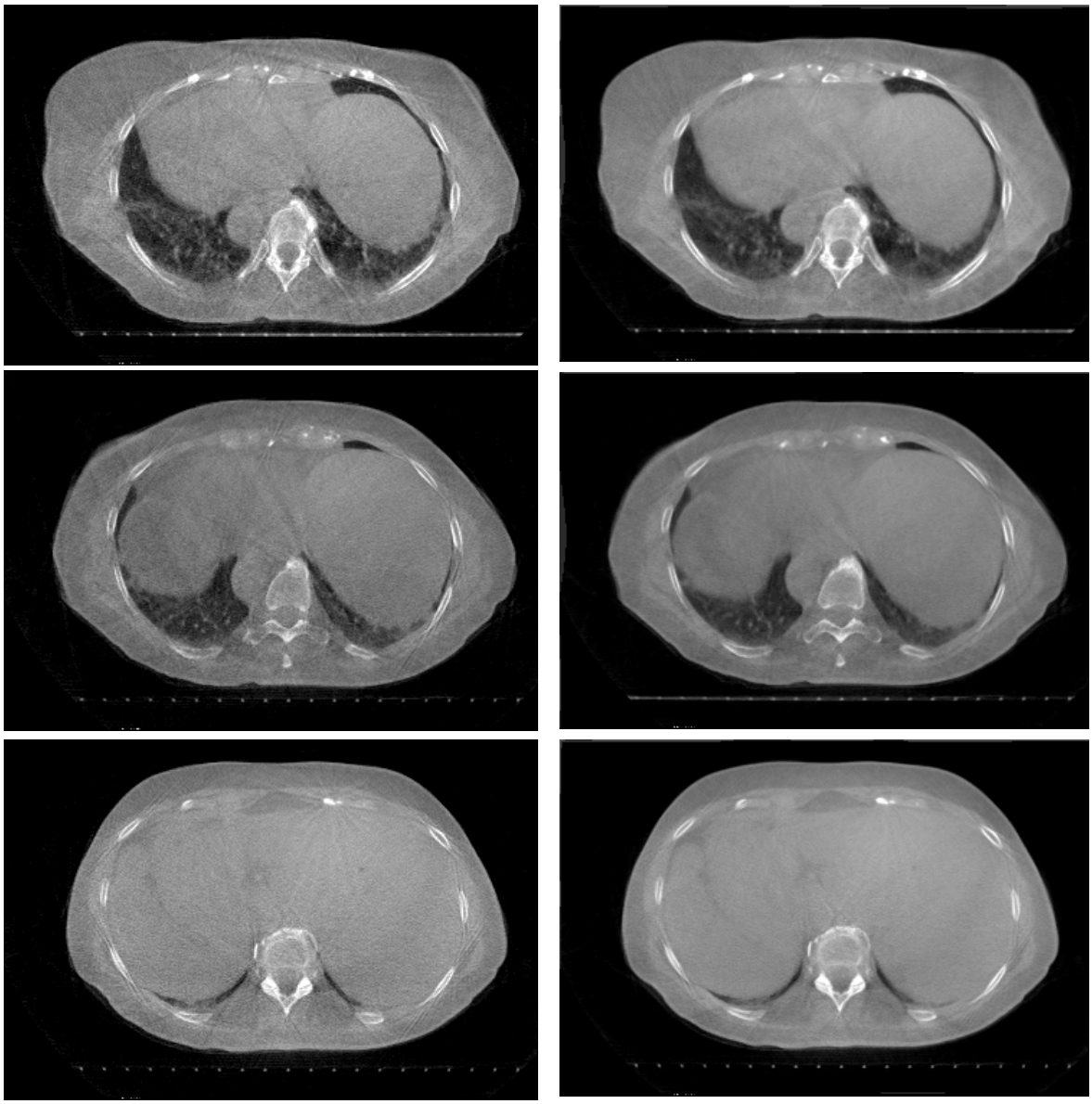

Figure 4.